nature medicine

FoxA1 directs the lineage and immunosuppressive properties of a novel regulatory T cell population in EAE and MS

Yawei Liu[1], Robert Carlsson[1], Manuel Comabella[2], JunYang Wang[1], Michael Kosicki[1], Belinda Carrion[1], Maruf Hasan[1], Xudong Wu[1], Xavier Montalban[2], Morten Hanefeld Dziegiel[3], Finn Sellebjerg[4], Per Soelberg Sørensen[4], Kristian Helin[1] & Shohreh Issazadeh-Navikas[1]

The defective generation or function of regulatory T (T_{reg}) cells in autoimmune disease contributes to chronic inflammation and tissue injury. We report the identification of FoxA1 as a transcription factor in T cells that, after ectopic expression, confers suppressive properties in a newly identified T_{reg} cell population, herein called FoxA1$^+$ T_{reg} cells. FoxA1 bound to the *Pdl1* promoter, inducing programmed cell death ligand 1 (Pd-l1) expression, which was essential for the FoxA1$^+$ T_{reg} cells to kill activated T cells. FoxA1$^+$ T_{reg} cells develop primarily in the central nervous system in response to autoimmune inflammation, have a distinct transcriptional profile and are CD4$^+$FoxA1$^+$CD47$^+$CD69$^+$PD-L1^{hi}FoxP3$^-$. Adoptive transfer of stable FoxA1$^+$ T_{reg} cells inhibited experimental autoimmune encephalomyelitis in a FoxA1–and Pd-l1–dependent manner. The development of FoxA1$^+$ T_{reg} cells is induced by interferon-β (IFN-β) and requires T cell–intrinsic IFN-α/β receptor (Ifnar) signaling, as the frequency of FoxA1$^+$ T_{reg} cells was reduced in *Ifnb*$^{-/-}$ and *Ifnar*$^{-/-}$ mice. In individuals with relapsing-remitting multiple sclerosis, clinical response to treatment with IFN-β was associated with an increased frequency of suppressive FoxA1$^+$ T_{reg} cells in the blood. These findings suggest that FoxA1 is a lineage-specification factor that is induced by IFN-β and supports the differentiation and suppressive function of FoxA1$^+$ T_{reg} cells.

Immune function that preserves tolerance while retaining antimicrobial function is imperative for preventing chronic inflammation and autoimmunity. T_{reg} cell–mediated immune suppression is important for suppressing inflammatory responses, and defects in the generation or function of T_{reg} cells are associated with autoimmune diseases[1].

T cell differentiation into effector or T_{reg} cells is determined by lineage-determining transcription factors. T-bet, GATA3 and ROR-γt promote the development and function of T helper type 1 (T_H1), T_H2 and T_H17 cells, respectively. FoxP3 is a lineage-determining transcription factor for natural and induced T_{reg} (n/iT_{reg}) cells[1–3]. In mice and humans, FOXP3 mutations lead to multiorgan failure and systemic autoimmunity[4,5].

T_{reg} cell defects have been reported in experimental autoimmune encephalomyelitis (EAE)[6], a tissue-specific inflammatory disease affecting the central nervous system (CNS) and a model of multiple sclerosis (MS). Neuron-induced, FoxP3-expressing T_{reg} cells control CNS inflammation in EAE[7]. However, the role of these cells in MS is under debate[8,9]. Although T_{reg} cell numbers are unchanged in MS, their suppressive function may be reduced, and the effects of IFN-β, a leading treatment for MS, on T_{reg} cell function remains contentious[8–12].

Mice lacking genes for *Ifnb* (*Ifnb*$^{-/-}$) or the *Ifn-a/b* receptor (*Ifnar*$^{-/-}$) develop chronic inflammatory and demyelinating EAE[13,14]. However, chronic relapsing-remitting EAE (RR-EAE) in *Ifnb*$^{-/-}$ mice is prevented by inducing T_{reg} cell expansion[15]. We previously reported that endogenous IFN-β regulates EAE not through effects on T cell priming and/or effector cytokine production, T_H cell differentiation, B cell activation or antibody production but rather by limiting CNS inflammation[13,16]. Although peripheral T_{reg} cell development and suppressive function are not impaired in *Ifnb*$^{-/-}$ mice, the development of tissue-resident T_{reg} cells in the inflamed CNS may be altered. We investigated whether chronic RR-EAE in *Ifnb*$^{-/-}$ mice results from a failure to generate tissue-specific T_{reg} cells.

We found no defects associated with FoxP3$^+$ T_{reg} cells in the inflamed CNS of *Ifnb*$^{-/-}$ mice. However, we discovered a previously undescribed population of T_{reg} cells in wild-type mice that was absent in *Ifnb*$^{-/-}$ mice. These suppressive cells, which we have termed FoxA1$^+$ T_{reg} cells, were generated in patients with relapsing-remitting MS (RRMS) that were responsive to treatment with IFN-β. FoxA1$^+$ T_{reg} cells express FoxA1 (hepatocyte nuclear factor 3α, also called HNF3α), a transcription factor[17] that is important in embryonic development, stem cell differentiation, hepatocyte development and cancer epigenetics[18–22]. FoxA1 is central in maintaining functional homeostasis of several postembryonic tissues, including those of the pancreas and brain. FoxA1 is also necessary for regulation of bile duct epithelial cell

[1]Biotech Research and Innovation Centre (BRIC), University of Copenhagen, Copenhagen, Denmark. [2]Centre d'Esclerosi Múltiple de Catalunya (CEM-Cat), Unitat de Neuroimmunologia Clínica, Hospital Universitari Vall d´Hebron (HUVH)–Universitat Autònoma de Barcelona, Barcelona, Spain. [3]Blood Bank, Copenhagen University Hospital, Copenhagen, Denmark. [4]Danish Multiple Sclerosis Center, University of Copenhagen and Department of Neurology, Rigshospitalet, Copenhagen, Denmark. Correspondence should be addressed to S.I.-N. (shohreh.issazadeh@bric.ku.dk).

Received 30 September 2013; accepted 22 January 2014; published online 16 February 2014; doi:10.1038/nm.3485

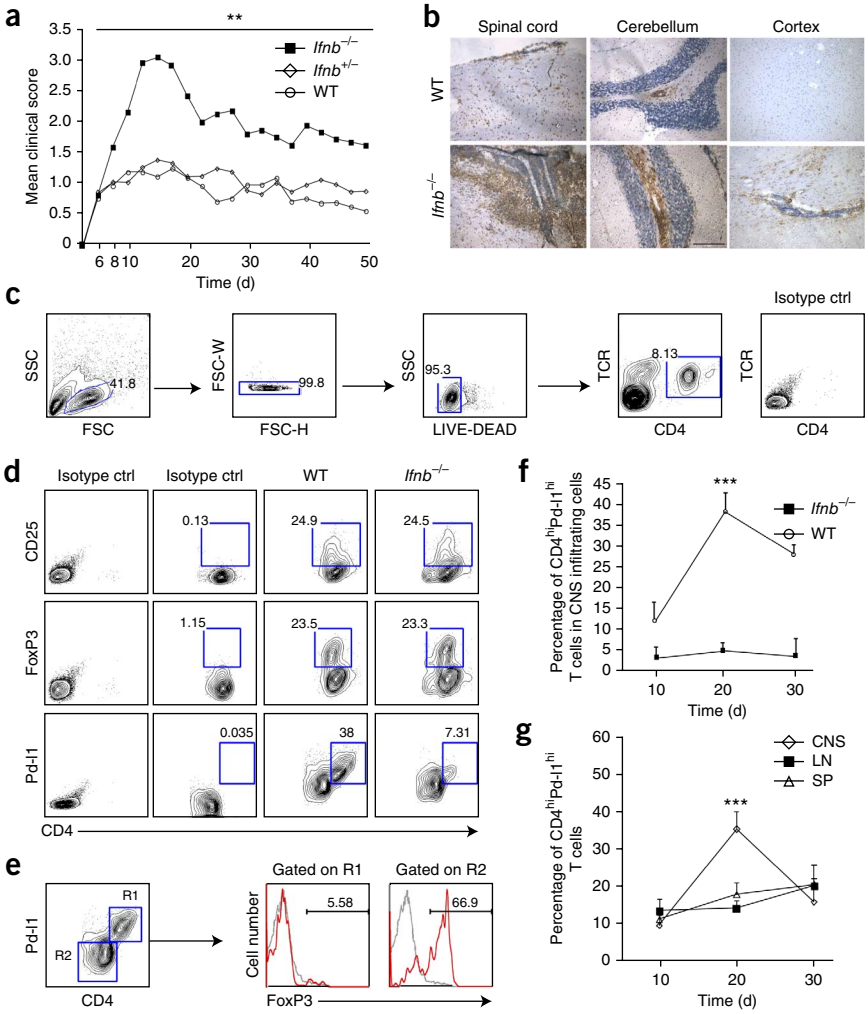

Figure 1 $CD4^{hi}Pd\text{-}l1^{hi}$ T cells are absent in the inflamed CNS of *Ifnb*$^{-/-}$ mice. (**a**) Clinical scores in *Ifnb*$^{-/-}$, *Ifnb*$^{+/-}$ and WT mice after the induction of RR-EAE using MBP_{89-101}. The data shown are the mean from two independent experiments (n (WT) = 21 mice, n (*Ifnb*$^{-/-}$) = 20 mice, n (*Ifnb*$^{+/-}$) = 21 mice). $^{**}P < 0.01$, one-way analysis of variance (ANOVA) Kruskal-Wallis test with multiple comparisons. (**b**) Spinal cord and brain cryosections from *Ifnb*$^{-/-}$ and WT mice show TCR-β^+ infiltrating cells (brown) and hematoxylin counterstaining (blue). Micrographs represent three individuals in each group. Scale bar, 100 µm. (**c**) FACS gating strategy for the isolation of $TCR\beta^+CD4^+$ T cells shown in **d**–**g**. SSC, side scatter; FSC, forward scatter; FSC-W, forward scatter width; FSC-H, forward scatter height; LIVE-DEAD, gating on cells that are alive versus dead; ctrl, control. (**d**) The numbers of $CD4^{hi}Pd\text{-}l1^{hi}$ T cells and T_{reg} ($CD4^+CD25^+FoxP3^+$) cells in WT and *Ifnb*$^{-/-}$ mice 20 d after EAE induction. (**e**) CNS-infiltrating $CD4^{hi}Pd\text{-}l1^{hi}$ T cells (R1 gated) are $FoxP3^-$. $CD4^+Pd\text{-}l1^{lo}$ cells (R2 gated) express FoxP3. The data shown (**c**–**e**) represent three independent experiments. (**f**) Percentage of $CD4^{hi}Pd\text{-}l1^{hi}$ T cells in the CNS infiltrating cells of WT and *Ifnb*$^{-/-}$ mice 10, 20 and 30 d after the induction of RR-EAE. (**g**) Percentage of $CD4^{hi}Pd\text{-}l1^{hi}$ T cells in the inflamed CNS, draining lymph nodes (LN) and spleen (SP) of WT mice after the induction of EAE. The data shown (**f**,**g**) are the mean ± s.d. from two independent experiments; each sample was pooled from two CNS tissues (total 20 mice, sample size of 10) for FACS staining. $^{***}P < 0.001$, two-way ANOVA with Tukey's multiple comparisons test.

proliferation and mediates lineage specification[23,24]. Previously, no function had been reported for FoxA1 in T cells. Here we demonstrate that FoxA1 is a lineage-specification factor that defines $FoxA1^+$ T_{reg} cells and directs the function of these T_{reg} cells.

RESULTS

$CD4^{hi}Pd\text{-}l1^{hi}$ T_{reg} cells develop in the CNS of EAE mice

We hypothesized that defects in tissue-specific T_{reg} cell development may contribute to the severe RR-EAE in *Ifnb*$^{-/-}$ mice. We used myelin basic protein $(MBP)_{89-101}$–induced EAE, which is a chronic demyelinating RR-EAE[13], as a model of RRMS. *Ifnb*$^{-/-}$ mice develop chronic EAE characterized by worse clinical scores, more relapses and increased CNS inflammation than wild-type (WT) littermates (**Fig. 1a**, **Supplementary Fig. 1a–c** and **Supplementary Table 1**). In addition to spinal cord and cerebellar inflammation, *Ifnb*$^{-/-}$ mice also develop cortical inflammation, a feature that is seen in early MS[25] and was absent in WT mice (**Fig. 1b**).

We found no differences in T_{reg} ($CD4^+CD25^+FoxP3^+$) cell numbers in the CNS of *Ifnb*$^{-/-}$ compared to WT mice with EAE (**Fig. 1d** and **Supplementary Fig. 2a**,**b**). T_{reg} cells from *Ifnb*$^{-/-}$ and WT mice were equally suppressive *in vitro* and reduced clinical scores *in vivo* when transferred to mice with EAE (**Supplementary Fig. 2c–e**). However, we consistently found a population of $CD4^{hi}Pd\text{-}l1^{hi}FoxP3^-$ T cells in the CNS of WT mice with EAE that was lacking in *Ifnb*$^{-/-}$ mice (**Fig. 1c–f**). $CD4^{hi}Pd\text{-}l1^{hi}$ T cells were enriched in the CNS of WT mice with RR-EAE as compared to the spleen or lymph nodes, and their frequency peaked 20 d after the induction of EAE (**Fig. 1g**). We hypothesized that these cells may suppress inflammation after the induction of EAE and that their absence in *Ifnb*$^{-/-}$ mice contributed to disease chronicity.

FoxA1 is a unique transcription factor in $FoxA1^+$ T_{reg} cells

We established an *ex vivo* primary encephalitogenic MBP_{89-101}–reactive T cell line (EncT) that was capable of inducing EAE after adoptive transfer into mice[13]. Hyperactivation of $CD8^+$ T cells results in the generation of $PD\text{-}1^{hi}CD8^+$ T cells in HIV-infected patients, which is dependent on PD-L1–PD-1 signaling[26]. We examined whether hyperactivation of EncT cells using multiple-antigen activation would generate $CD4^{hi}Pd\text{-}l1^{hi}$ cells. Multiple activation rounds with recall antigen (MBP_{89-101}, four to ten rounds) did not generate $CD4^{hi}Pd\text{-}l1^{hi}$ cells, but coculture of EncT cells with cerebellar granular neurons (CGNs), which also induces transforming growth factor-β (Tgf-β)$^+FoxP3^+$ T_{reg} cells[7] (**Supplementary Fig. 2f**) and regulates CNS immune homeostasis[27], led to the generation of $CD4^{hi}Pd\text{-}l1^{hi}$ T cells (**Fig. 2a**).

We compared the expression profile of these $CD4^{hi}Pd\text{-}l1^{hi}$ cells generated after coculture with CGNs to those of EncT cell progenitors and CGN-induced T_{reg} cells. Compared to EncT progenitors, 415 genes were uniquely upregulated in $CD4^{hi}Pd\text{-}l1^{hi}$ T cells and 451 were uniquely expressed in T_{reg} cells; 464 genes were uniquely downregulated in $CD4^{hi}Pd\text{-}l1^{hi}$ T cells and 483 were uniquely

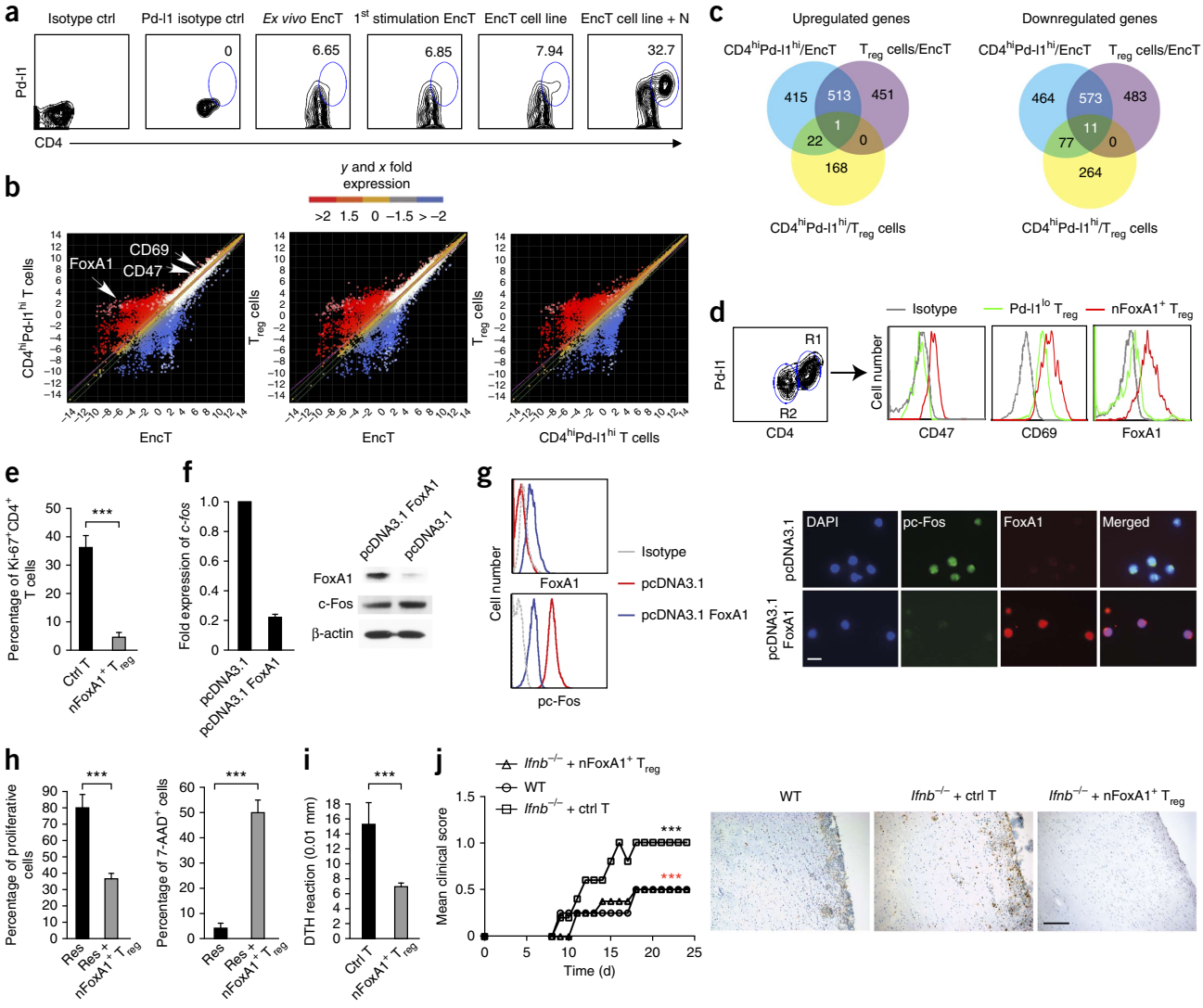

Figure 2 FoxA1$^+$ T_{reg} cells have a distinct transcriptional profile and suppress skin and CNS inflammation. (**a**) Representative FACS dot plots of CD4^{hi}Pd-l1^{hi} T cell generation after coculture of $MBP_{89–101}$–reactive EncT cells with CGNs. The results shown represent direct *ex vivo* culture of EncT cells isolated from EAE mice or culture of these cells after 48 h of stimulation with recall antigen (first stimulation EncT cells), multiple re-stimulations with antigen-loaded APCs for 96 h (EncT cell line) or after coculture with CGNs (EncT cell line + N). The data shown are from four independent experiments. (**b**) Signal intensity scatter plots from mouse Affymetrix 430 2.0 arrays hybridized with RNA from EncT cells alone or FACSAria-purified CD4^{hi}Pd-l1^{hi} T cells and T_{reg} (CD4$^+$CD25$^+$ and membrane-bound Tgf-β$^+$) cells after coculture with CGNs. Signal intensities (log_2) were analyzed by unpaired two-tailed Student's *t* test for independent triplicates filtered for 95% confidence of differential gene expression ($P \leq 0.05$). (**c**) Venn diagrams representing transcriptional similarities and differences between EncT progenitors, CD4^{hi}Pd-l1^{hi} T cells and T_{reg} cells. One ChannelGUI was used for the analysis of Affymetrix probe sets determined by upregulation or downregulation of at least ≥1.5-fold or ≤0.67-fold, respectively, at $P \leq 0.05$. Slashes indicate the comparison being made (e.g., CD4^{hi}Pd-l1^{hi}/EncT indicates CD4^{hi}Pd-l1^{hi} cells compared to EncT cells). Unpaired two-tailed Student's *t* test was used to analyze independent triplicates. (**d**) FACS analysis showing CD47, CD69 and nuclear FoxA1 expression in CD4^{hi}Pd-l1^{hi} (R1 gated; FoxA1$^+$ T_{reg}) cells and CD4$^+$Pd-l1^{lo} (R2 gated; Pd-l1^{lo} T) cells. The data shown are representative of three independent experiments. (**e**) Ki-67 expression (as assessed by FACS analysis) in FoxA1$^+$ T_{reg} cells (R1 gated) as compared to control cells (R2 gated). The data shown are the mean ± s.d. of three independent experiments. ***$P < 0.001$, unpaired two-tailed Student's *t* test. (**f**) Real-time PCR of *c-fos* expression. The data shown are the mean ± s.d. of duplicates. One representative result is shown from two independent experiments (left), and one representative western blot is shown from two independent experiments (right). (**g**) FACS of FoxA1 and pc-Fos expression (left). Representative data are from three independent experiments. Representative fluorescent immunocytochemistry (FLIC) micrographs of pc-Fos and FoxA1 localization in the nucleus in pcDNA3.1 FoxA1–transfected FoxA1$^+$ T_{reg} cells as compared to pcDNA3.1 control–transfected cells (right). Scale bar, 10 μm. The micrographs represent one out of four independent experiments (right). (**h**) Cell proliferation measured by CFSE dilution (left) and cell death assessed by 7-aminoactinomycin D (7-AAD) staining (right) of CFSE-labeled purified CD4$^+$ T cells that were activated with anti-CD3 for 24 h before coculture. These activated CFSE-labeled responder T cells (Res) were cocultured with purified nFoxA1$^+$ T_{reg} cells for an additional 24 h before analysis. The data shown are the mean ± s.d. from three independent experiments. ***$P < 0.001$, unpaired two-tailed Student's *t* test. (**i**) Delayed-type hypersensitivity (DTH), as measured by ear thickness, 48 h after injection of FoxA1$^+$ T_{reg} and control T cells (ctrl T; activated $MBP_{89–101}$ T cells). The data shown are representative of three independent experiments. Bars show the means ± s.d. of 3 mice. ***$P < 0.001$, unpaired two-tailed Student's *t* test. (**j**) Mean clinical scores (left) and H&E staining showing inflammatory cell recruitment in the spinal cord (right) of WT and *Ifnb*$^{-/-}$ mice after the injection of 2×10^6 $MBP_{89–101}$–specific EncT cells co-transferred with either 2×10^6 purified nFoxA1$^+$ T_{reg} cells or control T cells. The data shown are the mean clinical score from five mice. ***$P < 0.001$, one-way ANOVA Kruskal-Wallis test with multiple comparisons (left). Micrographs represent one out of three individuals in each group. Scale bar, 100 μm (right).

downregulated in T_{reg} cells. Compared to T_{reg} cells, $CD4^{hi}Pd\text{-}l1^{hi}$ T cells upregulated 168 genes and downregulated 264 genes. Compared to the EncT progenitors, the absolute number of genes constrained to $CD4^{hi}Pd\text{-}l1^{hi}$ or T_{reg} cells was equal; thus, these profiles indicate two distinct cell types (**Fig. 2b**,**c**). FoxA1, a protein that is critical for epigenetic reprogramming and cell-lineage commitment[24], was robustly upregulated in $CD4^{hi}Pd\text{-}l1^{hi}$ T cells compared to EncT cells (**Fig. 2b** and **Supplementary Table 2**). *FoxA1* was the first-ranked transcription factor using Gene Ontology (**Supplementary Fig. 3a**) and the top-ranked over-represented canonical pathway by Gene Set

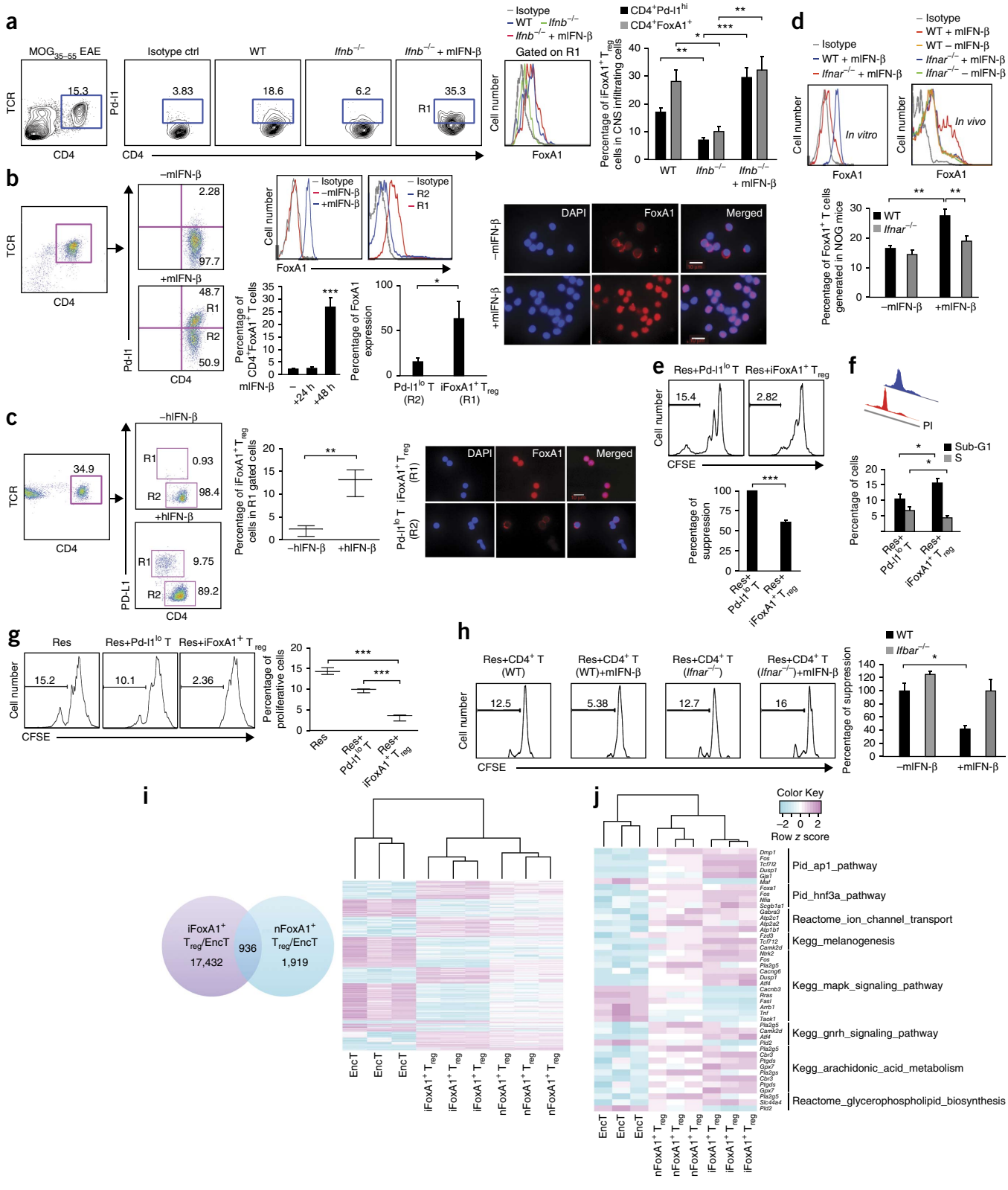

Enrichment Analysis (GSEA) compared to EncT cells (**Supplementary Table 3**), suggesting its involvement in the initiation of a specific gene expression program. $CD4^{hi}Pd\text{-}l1^{hi}$ T cells expressed CD47, CD69 and high levels of nuclear FoxA1 (**Fig. 2d** and **Supplementary Table 4**); hence, we named these cells $FoxA1^+$ T_{reg} cells. By comparing gene expression profiles and cell surface marker expression, we found that the neuron-induced $FoxA1^+$ (nFoxA1$^+$) T_{reg} cell profile (**Supplementary Fig. 3b**) was distinct from those of natural and Tgf-β–induced T_{reg} (n/iT_{reg}) cells[28–31] (**Supplementary Fig. 3c–e** and **Supplementary Tables 3–5**) and exhausted T cells[32] (**Supplementary Fig. 4** and **Supplementary Table 6**). We therefore examined *in vitro* and *in vivo* properties of the $FoxA1^+$ T_{reg} cell population.

$FoxA1^+$ T_{reg} cells suppress T cell activation and inflammation

Unlike CGN-induced T_{reg} cells[7] and their EncT progenitors, nFoxA1$^+$ T_{reg} cells were nonproliferative, as measured by expression of Ki-67 (**Fig. 2e**). We investigated signaling associated with FoxA1, in particular, nuclear translocation of phosphorylated c-Fos (pc-Fos), as c-Fos is involved in T cell proliferation and possibly T lymphocyte development and function[33]. Ectopic expression of FoxA1 in purified naive mouse $CD4^+$ T cells downregulates c-Fos expression (**Fig. 2f**), results in its translocation to the nucleus and reduces nuclear pc-Fos levels (**Fig. 2g**), suggesting that $FoxA1^+$ T_{reg} cells are nonproliferative and FoxA1 influences c-Fos signaling.

After coculture with anti-CD3 activated mouse $CD4^+$ responder T (ResT) cells, nFoxA1$^+$ T_{reg} cells (derived from $MBP_{89–101}$–reactive EncT cells cocultured with CGNs) inhibited proliferation and increased cell death of anti-CD3 activated ResT cells (**Fig. 2h**). nFoxA1$^+$ T_{reg} cells generated by coculturing of ovalbumin (OVA)-activated $CD4^+$ OT-II cells with CGNs also suppressed anti-CD3 and anti-CD28 activated ResT cells. Interleukin-2 (Il-2) rescued ResT cell proliferation but not cell death in nFoxA1$^+$ T_{reg} cell and Res T cell cocultures, indicating that $FoxA1^+$ T_{reg} cells regulated these events independently (**Supplementary Fig. 5**).

To investigate whether $FoxA1^+$ T_{reg} cells are suppressive *in vivo*, we adoptively transferred purified nFoxA1$^+$ T_{reg} cells intradermally to ears in a mouse delayed-type hypersensitivity model of tissue inflammation. Ears receiving nFoxA1$^+$ T_{reg} cells had significantly reduced swelling (**Fig. 2i**). Adoptive transfer of nFoxA1$^+$ T_{reg} cells together with encephalitogenic T cells also significantly reduced the incidence, clinical scores and severity of CNS inflammation of adoptive EAE in $Ifnb^{-/-}$ mice (**Fig. 2j** and **Supplementary Table 7**). These results suggest that $FoxA1^+$ T_{reg} cells exhibit suppressive function *in vivo*.

$FoxA1^+$ T_{reg} cells are induced by IFN-β and IFNAR signaling

As $Ifnb^{-/-}$ mice lack $FoxA1^+$ T_{reg} cells, we investigated whether treatment with IFN-β promotes $FoxA1^+$ T_{reg} cell development *in vivo*. $Ifnb^{-/-}$ mice develop severe myelin oligodendrocyte glycoprotein $(MOG)_{35–55}$–induced EAE, and IFN-β treatment reduces clinical symptoms in EAE[15]. Treatment of $Ifnb^{-/-}$ mice with mouse IFN-β (mIFN-β) increased the frequency of $FoxA1^+$ T_{reg} cells in the CNS (**Fig. 3a**) and spleen (**Supplementary Fig. 6**).

Treatment of purified $CD4^+$ T cells with mIFN-β induced T cell receptor-αβ (TCR-αβ)$^+CD4^{hi}Pd\text{-}l1^{hi}FoxA1^+$ T cells *in vitro*, which we refer to as IFN-β–induced $FoxA1^+$ (iFoxA1$^+$) T_{reg} cells. Compared to $Pd\text{-}l1^{lo}$ T cells, only $Pd\text{-}l1^{hi}$ T cells expressed nuclear FoxA1. Immunocytochemistry revealed nuclear FoxA1 expression after stimulation with mIFN-β (**Fig. 3b**).

We purified $CD4^+$ T cells from peripheral blood mononuclear cells (PBMCs) of healthy donors and cultured them with or without human IFN-β (hIFN-β). Treatment with hIFN-β did not induce FOXP3 or IL-35 expression, which are markers of classical T_{reg} cells, or $PD\text{-}1^{hi}$, which is upregulated in exhausted T cells (**Supplementary Fig. 7a–d**). However, hIFN-β induced TCR-αβ$^+CD4^+PD\text{-}L1^{hi}FoxA1^+$ T_{reg} cells. Purified $PD\text{-}L1^{hi}$ (R1 gated; iFoxA1$^+$ T_{reg} cells) expressed FoxA1, which localized to the nucleus, as compared to $PD\text{-}L1^{lo}$ T cells (R2 gated) (**Fig. 3c**).

We next studied whether iFoxA1$^+$ T_{reg} cell generation required IFN-β receptor signaling. *In vitro* treatment of $CD4^+$ T cells purified from $Ifnar^{-/-}$ mice with mIFN-β did not increase the expression of FoxA1 or the proportion of $FoxA1^+$ cells (**Fig. 3d**). To determine the requirement for IFN-β–IFNAR signaling in $FoxA1^+$ T_{reg} cell generation *in vivo* and whether IFN-β acts in a T cell–intrinsic manner or relies on other cells, we purified $CD4^+$ T cells from $Ifnar^{-/-}$ and WT mice and transferred them intravenously (i.v.) to NOG mice. mIFN-β promoted the generation of $FoxA1^+$ T_{reg} cells in mice receiving WT

Figure 3 $FoxA1^+$ T_{reg} cells are induced by IFN-β. (**a**) Representative FACS dot plots of $CD4^+Pd\text{-}l1^{hi}$ cells (left), a histogram of R1-gated ($CD4^+FoxA1^+$) cells (middle) and quantification of CNS $FoxA1^+$ T_{reg} cells (right) in mice with $MOG_{35–55}$–induced EAE. The data shown are the mean ± s.d. ($n = 5$ per group). $^*P < 0.05$, $^{**}P < 0.01$, $^{***}P < 0.001$, one-way ANOVA with Newman-Keuls *post hoc* test for multiple comparison correction. (**b**) Representative FACS dot plots gated onTCR-αβ$^+CD4^+Pd\text{-}l1^{hi}$ T cells (left), a FACS histogram of FoxA1 expression (upper middle) (one of three different experiments) and quantification of $FoxA1^+CD4^+$ T cells (lower middle). The data shown are the mean ± s.d. from three different experiments. $^*P < 0.05$, $^{***}P \leq 0.001$, unpaired two-tailed Student's *t* test. Representative FLIC micrographs of nuclear localization of FoxA1 (right). Micrographs represent one out of four individuals per group. Scale bars, 10 μm (right). (**c**) Representative FACS dot plots (left) and quantification of human IFN-β–induced TCR-αβ$^+CD4^+PD\text{-}L1^{hi}FoxA1^+$ T_{reg} cells *in vitro*. Horizontal lines indicate the mean ± s.d. $^{**}P \leq 0.01$, Student's unpaired *t* test. $n = 4$ (middle). Representative FLIC micrographs (one out of four individuals per group) of FoxA1 expression and nuclear localization in purified TCR-αβ$^+CD4^+PD\text{-}L1^{hi}FoxA1^+$ T_{reg} cells (R1 gated) and $FoxA1^-$ T cells (R2 gated). Scale bar, 10 μm (right). (**d**) A FACS histogram of FoxA1 expression (left) and a FACS histogram and quantification of *in vivo*–generated $FoxA1^+$ in splenocytes (right). Bars indicate the mean ± s.d. ($n = 3$ mice per group). $^{**}P < 0.01$, one-way ANOVA with Newman-Keuls *post hoc* test for multiple comparison correction. (**e**) Representative FACS histogram (top) and the percentage of suppression (bottom) in CFSE-labeled activated $CD4^+$ T cells (Res) cocultured with hIFN-β–induced $FoxA1^+$ T_{reg} cells (R1 gated) and $CD4^+Pd\text{-}l1^{lo}$ T cells (R2 gated). Bars indicate the mean ± s.d. ($n = 3$). $^{***}P < 0.001$, unpaired two-tailed Student's *t* test. (**f**) Representative FACS histogram of propidium iodide (PI) staining (top) and the quantified percentages of ResT cells in the various cell cycle phases (bottom). Bars indicate the mean ± s.d. ($n = 3$). $^*P < 0.05$, unpaired two-tailed Student's *t* test. (**g**) Representative FACS histogram of CFSE-labeled activated ResT cells cocultured with purified $iFoxA1^+$ T_{reg} cells (left) and their quantification. Bars indicate the mean ± s.d. ($n = 3$). $^{***}P < 0.001$, one-way ANOVA with Newman-Keuls *post hoc* test for multiple comparison correction (right). (**h**) Representative FACS histograms (left) and quantification of CFSE-labeled activated ResT cells in chimeric NOG mice. Bars indicate the mean ± s.d. ($n = 3$). $^*P < 0.05$, one-way ANOVA with Newman-Keuls *post hoc* test for multiple comparison correction (right). (**i**) Venn diagram of the overlap between differentially expressed probe sets that are upregulated and downregulated in the same direction in $iFoxA1^+$ T_{reg} compared to EncT cells and nFoxA1$^+$ T_{reg} cells compared to EncT cells (left). 936 common probe sets of $FoxA1^+$ T_{reg} cells as compared to EncT cells were compiled to determine the heatmap profile of the $FoxA1^+$ T_{reg} cells (right). (**j**) Heatmap of genes commonly regulated by $iFoxA1^+$ T_{reg} and nFoxA1$^+$ T_{reg} cells as compared to EncT cells that are involved in commonly regulated pathways, determined by GSEA. Data are from triplicates.

but not *Ifnar*$^{-/-}$ CD4$^+$ T cells (**Fig. 3d**), suggesting that the induction of FoxA1$^+$ T_{reg} cells by IFN-β *in vitro* and *in vivo* requires IFN-β receptor signaling in CD4$^+$ T cells.

We then studied the *in vitro* suppressive capacity of iFoxA1$^+$ T_{reg} cells. hIFN-β–induced FoxA1$^+$ T_{reg} cells reduced the proliferation of cocultured ResT cells, inhibited their entry into the S phase and induced ResT cell death in the sub-G1 population (**Fig. 3e**,**f**). Purified mIFN-β–induced FoxA1$^+$ T_{reg} cells were similarly suppressive (**Fig. 3g**). Using chimeric mice, we investigated whether *in vivo* IFN-β–generated FoxA1$^+$ T_{reg} cell–mediated suppression of activated ResT cells required IFN-β–IFNAR signaling. We observed suppression of ResT cells only in NOG mice receiving IFN-β–treated WT CD4$^+$ T cells but not in those receiving *Ifnar*$^{-/-}$ CD4$^+$ T cells (**Fig. 3h**), confirming that generation of suppressive FoxA1$^+$ T_{reg} cells required IFN-β–IFNAR signaling.

T_{reg} and T_H2 cells modulate antigen-presenting cells (APCs)[34], and effective IFN-β treatment of RRMS is associated with modulation of APC function[35,36]. IFN-β-induced IL-10 expression in APCs is associated with reduced MS symptoms[37]. In contrast to T_{reg} cells and T_H2 cells, human iFoxA1$^+$ T_{reg} cells did not induce IL-10 expression in cocultured APCs. However, iFoxA1$^+$ T_{reg} cells reduced the production of proinflammatory cytokines (IL-12 and IL-17) by APCs (**Supplementary Fig. 8**).

Gene expression profile homology between nT_{reg} cells and Tgf-β–induced T_{reg} (iT_{reg}) cells has been reported[28–31] (**Supplementary Fig. 3e**). To identify a gene expression signature characteristic of FoxA1$^+$ T_{reg} cells, we compared the gene expression profiles of nFoxA1$^+$ and iFoxA1$^+$ T_{reg} cells. As shown by a Venn diagram (**Fig. 3i**), 936 genes were similarly upregulated or downregulated in nFoxA1$^+$ and iFoxA1$^+$ T_{reg} cells. We compiled a list of genes commonly expressed by FoxA1$^+$ T_{reg} cells as compared to EncT cells to construct a heatmap profile of FoxA1$^+$ T_{reg} cells (**Fig. 3i**). Using Gene Ontology analysis, we found that *FoxA1* was among the top 20-ranking transcription factors differentially expressed in iFoxA1$^+$ T_{reg} cells (**Supplementary Table 8**). To identify common canonical signaling pathways, we analyzed the common 936 genes by GSEA. We tabulated genes in the top 20 pathways and compared them to find the overlap in known biological pathways (**Supplementary Tables 9** and **10**). We also generated a heatmap of the shared pathways (8/20) between i/nFoxA1$^+$ T_{reg} cells compared to EncT cells (**Fig. 3j**).

FoxA1 confers suppressive function in FoxA1$^+$ T_{reg} cells

We investigated whether FoxA1 is necessary for the development and suppressive activity of IFN-β–induced FoxA1$^+$ T_{reg} cells and sufficient to induce suppressive function in T_{reg} cells. We knocked down FoxA1 expression using FoxA1-specific siRNA (FoxA1KD) in purified CD4$^+$ T cells before stimulating them with mIFN-β (**Fig. 4a**). To prevent off-target effects, we used four different siRNAs targeting the 3′ untranslated region (UTR) region of *Foxa1*. As all of the siRNAs showed specific knockdown effects, we pooled them together (**Supplementary Fig. 9a**,**b**). siRNA-mediated silencing of FoxA1 expression reduced Pd-l1 expression in IFN-β–treated CD4$^+$ T cells (**Fig. 4a**) and resulted in a loss of suppressive function *in vitro* (**Fig. 4b**). We transferred carboxyfluorescein succinimidyl ester (CFSE)-labeled anti-CD3 preactivated ResT cells and co-transferred control siRNA–treated T cells or FoxA1 siRNA–treated T cells i.v. to chimeric NOG mice and co-injected them with mIFN-β. *In vivo* mIFN-β–treated CD4$^+$ T cells expressed FoxA1 (**Fig. 4c**, left). Whereas control siRNA– and mIFN-β–treated CD4$^+$ T cells (iFoxA1$^+$ T_{reg} cells) suppressed CFSE-labeled ResT cells, FoxA1 siRNA– and mIFN-β–treated CD4$^+$ T cells did not suppress ResT cell proliferation, as assessed by CFSE dilution (**Fig. 4c**, middle and right), indicating that FoxA1 is required for the suppressive activity of FoxA1$^+$ T_{reg} cells. FoxA1$^+$ T_{reg} cells generated by ectopically overexpressing FoxA1 in naive CD4$^+$ T cells (**Fig. 4d** and **Supplementary Fig. 9c**) reduced ResT cell proliferation (**Fig. 4d**), suggesting that FoxA1 confers suppressive function in FoxA1$^+$ T_{reg} cells.

FoxA1$^+$ T_{reg} cell suppression depends on FoxA1 and PD-L1

To assess the *in vivo* mechanisms of FoxA1$^+$ T_{reg} cell–mediated suppression, we co-transferred iFoxA1$^+$ T_{reg} cells and $MOG_{35–55}$–reactive encephalitogenic T cells to *Ifnb*$^{-/-}$ mice. Whereas iFoxA1$^+$ T_{reg} cells reduced clinical scores and CNS inflammation, silencing of FoxA1 expression in iFoxA1$^+$ T_{reg} cells reduced their suppressive function (**Fig. 4e** and **Supplementary Table 11**). In FoxA1KD cells, ectopic expression of siRNA-insensitive pcDNA3.1 FoxA1, which encodes the open reading frame (ORF) sequence of *Foxa1* (**Supplementary Fig. 9a**,**d**,**e**), was sufficient to restore the suppressive function of iFoxA1$^+$ T_{reg} cells. Silencing of Pd-l1 expression and administration of a Pd-l1–specific blocking antibody also reduced also the suppressive function of iFoxA1$^+$ T_{reg} cells (**Fig. 4e** and **Supplementary Table 11**). Though we removed the antibody prior to transferring the cells, any remaining Pd-l1–specific antibody could have affected the encephalitogenicity of cells.

We labeled iFoxA1$^+$ T_{reg} cells and all control variants with CFSE before transferring them to mice with adoptive EAE. Analysis of CFSE$^+$ T cells 20 or 40 days after transfer revealed that although iFoxA1$^+$ T_{reg} cells did not proliferate, the control T cells (control siRNA–treated and pcDNA3.1-treated activated T cells) and iFoxA1$^+$ T_{reg} cells in which either FoxA1 or Pd-l1 had been silenced proliferated *in vivo* (**Fig. 4f**). The phenotype of iFoxA1$^+$ T_{reg} cells was stable *in vivo*, as they maintained FoxA1 expression and did not upregulate FoxP3 expression up to 40 days after transfer (**Fig. 4g**,**h**). These results indicate that the suppressive function of FoxA1$^+$ T_{reg} cell *in vivo* is mediated by FoxA1 and Pd-l1.

FoxA1$^+$ T_{reg} cells induce caspase 3–mediated apoptosis

PD-L1 is involved in negative signaling to T cells and induces cell cycle arrest[38]. As iFoxA1$^+$ T_{reg} cell–dependent suppression of T cell proliferation is mediated by Pd-l1 (**Fig. 4e**), we sought to investigate how Pd-l1 in FoxA1$^+$ T_{reg} cells functioned. We found that in cocultures with nFoxA1$^+$ T_{reg} cells, antibody-mediated blockade of Pd-l1 restored ResT cell proliferation and inhibited cell death (**Fig. 5a**). PD-L1 binds to PD-1 and B7.1 (ref. 39). Antibody-mediated blockade of Pd-l1 and Pd-1 in coculture reduced nFoxA1$^+$ T_{reg} cell–induced apoptosis of ResT cells, but blocking B7.1 or B7.2 did not (**Fig. 5b**). PD-L1–PD-1–mediated suppression is also seen in human iFoxA1$^+$ T_{reg} cells, as siRNA-mediated silencing of PD-1 expression in human ResT cells abrogates the suppressive effects of iFoxA1$^+$ T_{reg} cells (**Fig. 5c**).

AKT phosphorylation (pAKT) promotes T cell activation. Human iFoxA1$^+$ T_{reg} cells reduce pAKT expression in ResT cells. This effect was dependent on PD-1 signaling, as silencing of PD-1 in ResT cells increased pAKT expression (**Fig. 5c** and **Supplementary Fig. 10a**). iFoxA1$^+$ T_{reg} cells also induce PD-1–dependent caspase 3 cleavage in ResT cells (**Fig. 5c** and **Supplementary Fig. 10b**). Phosphorylation of p38 (phospho-p38), a mitogen-activated protein kinase, regulates the cell cycle and apoptosis[40]. Phosphorylation of p38 MAPK was also regulated in a PD-1–dependent fashion, as silencing of PD-1 in ResT cells increased phospho-p38 in ResT cells after coculturing with human iFoxA1$^+$ T_{reg} cells (**Supplementary Fig. 10c**).

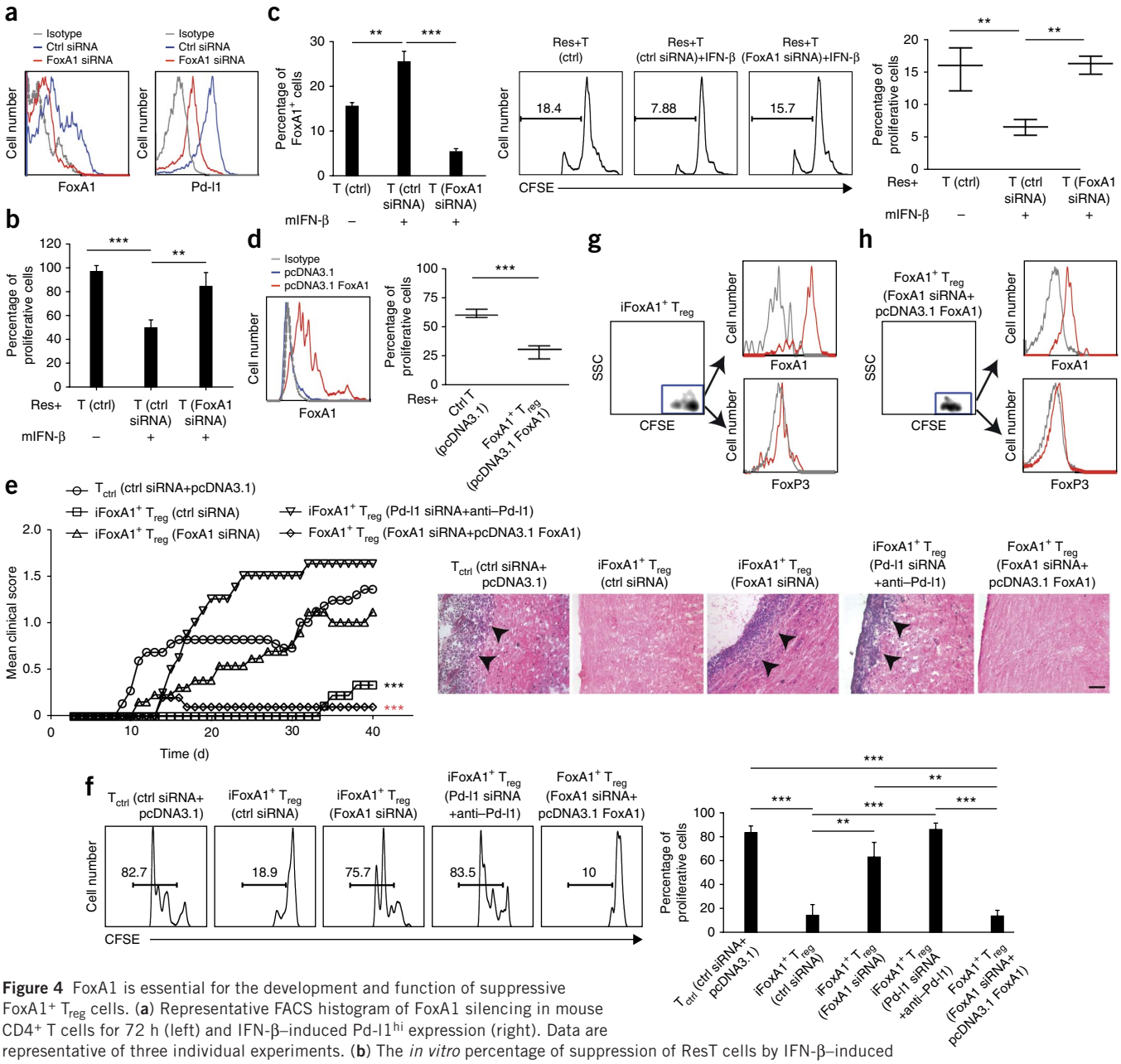

Figure 4 FoxA1 is essential for the development and function of suppressive FoxA1$^+$ T_{reg} cells. (**a**) Representative FACS histogram of FoxA1 silencing in mouse CD4$^+$ T cells for 72 h (left) and IFN-β–induced Pd-l1^{hi} expression (right). Data are representative of three individual experiments. (**b**) The *in vitro* percentage of suppression of ResT cells by IFN-β–induced FoxA1$^+$ T_{reg} cells with or without FoxA1 silencing, calculated as Res + CD4$^+$ T (control siRNA) + mIFN-β or Res + CD4$^+$ T (FoxA1 siRNA) + mIFN-β divided by Res + CD4$^+$ T (control) – mIFN-β multiplied by 100. Bars indicate the mean ± s.d. ($n = 3$). $^{**}P < 0.01$, $^{***}P < 0.001$, one-way ANOVA with Newman-Keuls *post hoc* test for multiple comparison correction. (**c**) FACS quantification of FoxA1$^+$ T_{reg} cells. Bars indicate the mean ± s.d. ($n = 3$ mice per group). $^{**}P < 0.01$, $^{***}P < 0.001$, one-way ANOVA with Newman-Keuls *post hoc* test for multiple comparison correction (left). Representative FACS histgrams of CFSE-labeled CD4$^+$ ResT cell proliferation in NOG mice receiving the indicated cells with or without mIFN-β (middle). The quantifications of these proliferative cells are shown as the mean ± s.d. ($n = 3$). $^{**}P < 0.01$, one-way ANOVA with Newman-Keuls *post hoc* test for multiple comparison correction (right). (**d**) A representative FACS histogram from four individual experiments shows FoxA1 expression (left). Suppressive function as shown by quantification of CFSE-labeled activated CD4$^+$ Res T cells cocultured with the indicated cells. Bars indicate the mean ± s.d. $^{***}P < 0.001$, Student's unpaired *t* test ($n = 3$; right). (**e**) The mean clinical scores of mice with $MOG_{35–55}$–induced EAE by adoptive transfer (left) and H&E micrographs of spinal cord sections (right) in *Ifnb*$^{-/-}$ mice receiving the indicated cells. Only groups that received iFoxA1$^+$ T_{reg} (IFN-β–treated control siRNA) and FoxA1$^+$ T_{reg} (pcDNA3.1 FoxA1) cells suppressed EAE, but not those receiving iFoxA1$^+$ T_{reg} (FoxA1 siRNA) or iFoxA1$^+$ T_{reg} (Pd-l1 siRNA and antibodies to Pd-l1) cells. The data shown are the mean from three independent experiments ($n = 22$, 9, 13, 8 and 10 mice in the respective groups). $^{***}P < 0.001$, iFoxA1$^+$ T_{reg} cells (control siRNA) compared to all control groups; $^{***}P < 0.001$, FoxA1$^+$ T_{reg} cells (FoxA1 siRNA + pcDNA3.1 FoxA1) compared to the respective control group, one-way ANOVA Kruskal-Wallis test with multiple comparisons (left). One representative micrograph of H&E staining per group (3–6 per group) illustrates the prevention of inflammatory cell infiltrates (arrows) in the spinal cords of mice treated with FoxA1$^+$ T_{reg} cells at day 40 after adoptive EAE. Scale bar, 100 µm (right). (**f**) Representative FACS histograms show proliferative CFSE$^+$-gated splenocytes (left). Also shown is quantification of CFSE$^+$ splenocytes 40 d after induction of EAE by adoptive transfer. Bars indicate the mean ± s.d. ($n = 5$ mice per group). $^{**}P < 0.01$, $^{***}P < 0.001$, one-way ANOVA with Newman-Keuls post test (right). (**g**,**h**) Representative gated CFSE-labeled iFoxA1$^+$$T_{reg}$ (IFN-β–induced control siRNA) cells (**g**) and FoxA1$^+$ T_{reg} (FoxA1 siRNA + pcDNA3.1 FoxA1) cells (**h**) show positive expression of FoxA1 but not FoxP3 at 40 d after adoptive transfer *in vivo*. Data are representative from six samples.

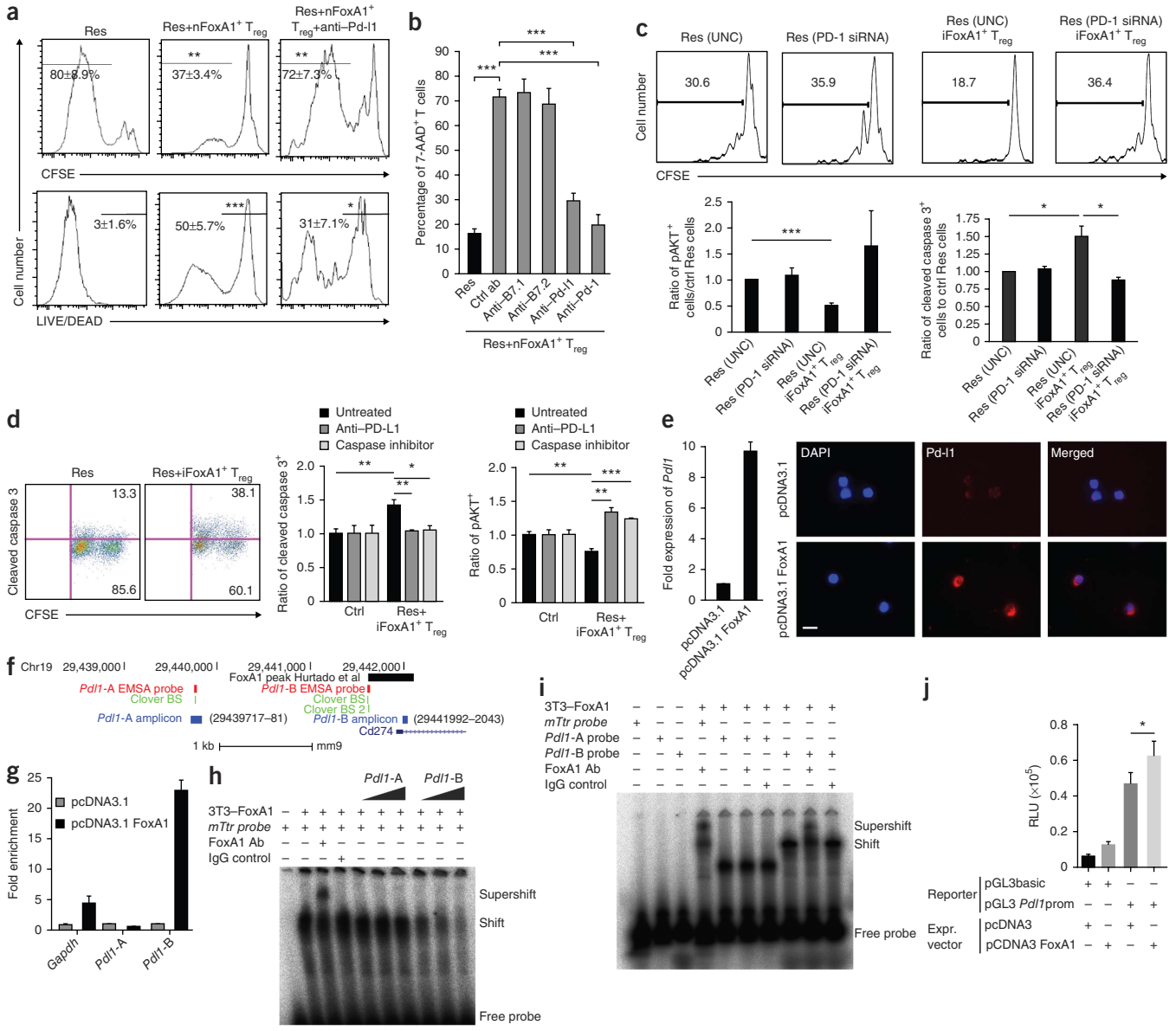

Figure 5 Ectopic FoxA1 expression generates suppressive FoxA1$^+$ T_{reg} cells that induce activated T cell apoptosis. (**a**) Representative FACS histograms of CFSE-labeled activated ResT cells cocultured with purified mouse nFoxA1$^+$ T_{reg} cells with or without antibodies to Pd-l1 (5 μg ml^{-1}). CFSE$^+$ shows cell proliferation (top), and LIVE/DEAD depicts cell death (bottom). Results are from one out of three experiments. Error bars, s.d. $^*P < 0.05$, $^{**}P < 0.01$, $^{***}P < 0.001$, Student's unpaired *t* test. (**b**) Quantification of 7-AAD$^+$ ResT cells after coculture with nFoxA1$^+$ T_{reg} cells with Pd-l1, Pd-1 (5 μg ml^{-1}), B7.1, B7.2 (10 μg ml^{-1}) or isotype control (10 μg ml^{-1}) antibodies (ab). The data shown are the mean ± s.d. of three independent experiments, $^{***}P < 0.001$, Student's unpaired *t* test. (**c**) Representative histograms of CFSE-labeled preactivated human ResT cells (treated with different siRNAs as indicated) that were cocultured with human IFN-β–induced (i)FoxA1$^+$ T_{reg} cells (top). The ratios of pAKT (bottom, left) and cleaved caspase 3 (bottom, right) in ResT cells are also shown relative to control Res T (UNC). Bars indicate the mean ± s.d. $^*P < 0.05$, $^{***}P < 0.001$, Student's unpaired *t* tests ($n = 3$). (**d**) Representative FACS dot plots (left) and quantification of cleaved caspase 3 (middle) and pAKT (right) in ResT cells cocultured with human iFoxA1$^+$ T_{reg} cells with a PD-L1–specific antibody (10 μg ml^{-1}) or the caspase inhibitor Z-VAD-FMK (4 μM). Bars indicate the mean ± s.d. $^*P < 0.05$, $^{**}P < 0.01$, $^{***}P < 0.001$, Student's unpaired *t* test ($n = 3$). (**e**) Quantitative PCR (qPCR) of *Pdl1* mRNA in mouse pcDNA3.1 FoxA1–transfected FoxA1$^+$ T_{reg} cells compared to pcDNA3.1 control–transfected cells. The data shown are the mean ± s.d. from duplicates (left). Also shown are representativeFLIC micrographs out of four individuals in each group. Scale bar, 10 μm (right). (**f**) The *Pdl1* locus. Shown are chromosome 19 upstream of *Pdl1* in the mouse genome (mm9) with *Pdl1*-A and *Pdl1*-B electrophoretic mobility shift assay (EMSA) probes and ChIP amplicons and the FoxA1 ChIP-seq peak in ZR751 cells converted to the mm9 assembly using LiftOver in UCSC from the hg18 assembly. FoxA1 binding sites were selected using Clover. (**g**) pcDNA3.1 FoxA1–transfected or control plasmid–transfected CD4$^+$ T cells analyzed by ChIP-qPCR of FoxA1-occupied DNA. Results are shown as a percentage of the input normalized for FoxA1 enrichment to IgG control. Data are representative of one of three comparable experiments. Bars indicate the mean ± s.d. from duplicates. (**h**) EMSA on nuclear extracts from FoxA1-transfected 3T3 cells using labeled *mTtr* positive control probe and increasing doses of competing *Pdl1*-A and *Pdl1*-B probes. (**i**) EMSA on nuclear extracts from FoxA1-transfected 3T3 cells with labeled *Pdl1*-A and *Pd-l1*-B probes. The data shown are representative of two independent experiments. (**j**) 3T3 cells were transfected with empty vector or *Pdl1* promoter reporter plasmids (pGL3basic and pGL3 *Pdl1*prom) and cotransfected with an empty mammalian expression vector (pcDNA3.1) or a FoxA1-containing expression (Expr.) vector (pcDNA3.1 FoxA1). The data shown are from one out of four independent experiments. The bar indicates the mean relative luciferase activity (RLU, relative to *Renilla* luciferase) with the s.d. $^*P < 0.05$, one-way ANOVA with Tukey's multiple testing correction.

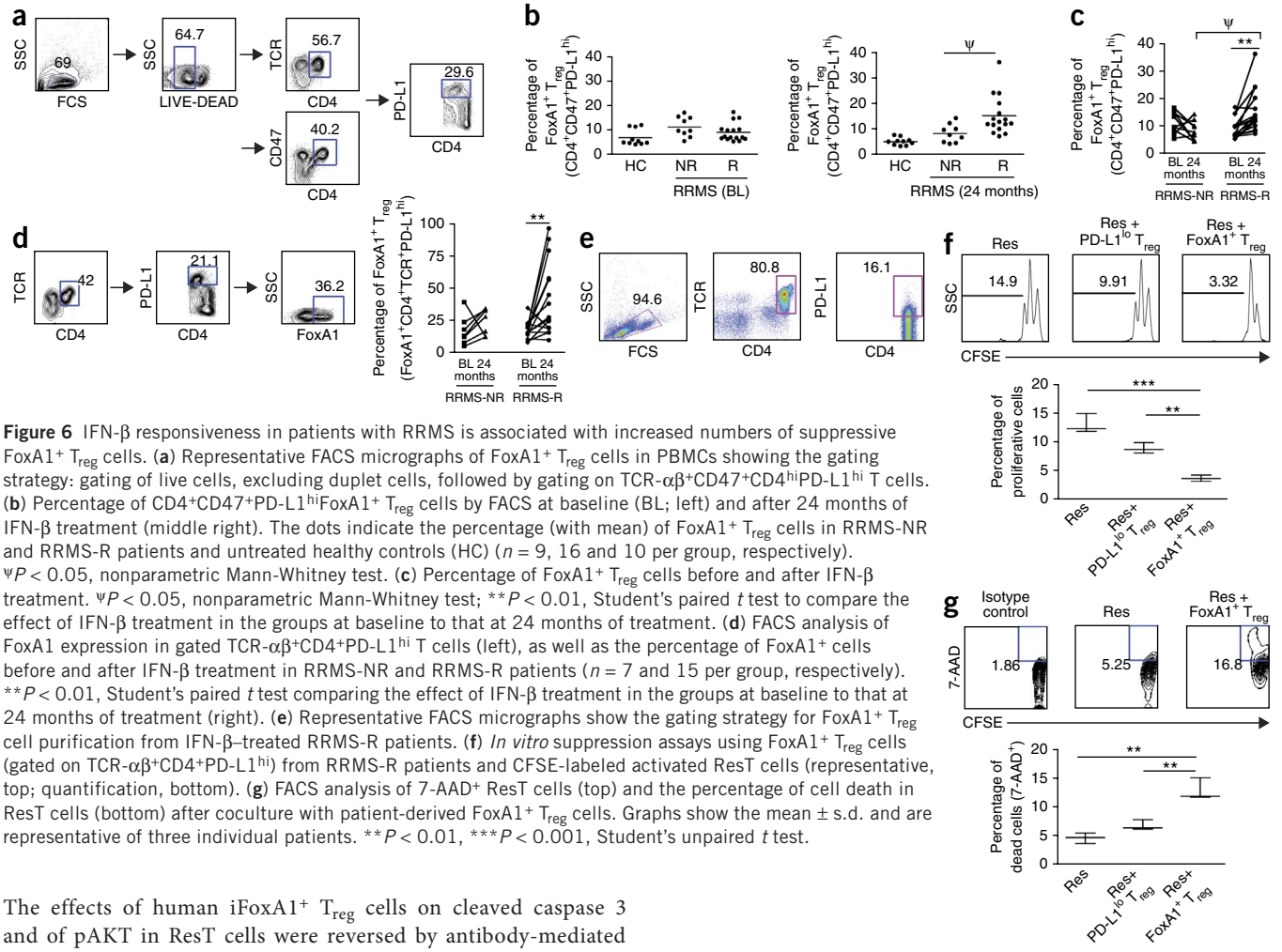

Figure 6 IFN-β responsiveness in patients with RRMS is associated with increased numbers of suppressive FoxA1$^+$ T_{reg} cells. (**a**) Representative FACS micrographs of FoxA1$^+$ T_{reg} cells in PBMCs showing the gating strategy: gating of live cells, excluding duplet cells, followed by gating on TCR-αβ$^+$CD47$^+$CD4^{hi}PD-L1^{hi} T cells. (**b**) Percentage of CD4$^+$CD47$^+$PD-L1^{hi}FoxA1$^+$ T_{reg} cells by FACS at baseline (BL; left) and after 24 months of IFN-β treatment (middle right). The dots indicate the percentage (with mean) of FoxA1$^+$ T_{reg} cells in RRMS-NR and RRMS-R patients and untreated healthy controls (HC) (n = 9, 16 and 10 per group, respectively). $\Psi P < 0.05$, nonparametric Mann-Whitney test. (**c**) Percentage of FoxA1$^+$ T_{reg} cells before and after IFN-β treatment. $\Psi P < 0.05$, nonparametric Mann-Whitney test; $^{**}P < 0.01$, Student's paired t test to compare the effect of IFN-β treatment in the groups at baseline to that at 24 months of treatment. (**d**) FACS analysis of FoxA1 expression in gated TCR-αβ$^+$CD4$^+$PD-L1^{hi} T cells (left), as well as the percentage of FoxA1$^+$ cells before and after IFN-β treatment in RRMS-NR and RRMS-R patients (n = 7 and 15 per group, respectively). $^{**}P < 0.01$, Student's paired t test comparing the effect of IFN-β treatment in the groups at baseline to that at 24 months of treatment (right). (**e**) Representative FACS micrographs show the gating strategy for FoxA1$^+$ T_{reg} cell purification from IFN-β–treated RRMS-R patients. (**f**) *In vitro* suppression assays using FoxA1$^+$ T_{reg} cells (gated on TCR-αβ$^+$CD4$^+$PD-L1^{hi}) from RRMS-R patients and CFSE-labeled activated ResT cells (representative, top; quantification, bottom). (**g**) FACS analysis of 7-AAD$^+$ ResT cells (top) and the percentage of cell death in ResT cells (bottom) after coculture with patient-derived FoxA1$^+$ T_{reg} cells. Graphs show the mean ± s.d. and are representative of three individual patients. $^{**}P < 0.01$, $^{***}P < 0.001$, Student's unpaired t test.

The effects of human iFoxA1$^+$ T_{reg} cells on cleaved caspase 3 and of pAKT in ResT cells were reversed by antibody-mediated blockade of PD-L1 or by utilizing Z-VAD-FMK, a general inhibitor of caspases (**Fig. 5d**).

FoxA1 binds the *Pdl1* promoter and upregulates Pd-l1

FoxA1 binds enhancer sequences in cancer cells[17] and controls *TTR* transcription[41]. We studied whether FoxA1 regulates Pd-l1 expression in T cells. FoxA1 overexpression resulted in markedly elevated Pd-l1 mRNA and protein expression in FoxA1$^+$ T_{reg} cells (**Fig. 5e**).

We next investigated whether FoxA1 regulates Pd-l1 in T cells through direct binding to a putative *Pdl1* promoter. On the basis of an unconfirmed peak in FoxA1 chromatin immunoprecipitation (ChIP) using a breast cancer cell line[17], we identified two potential binding sites: *Pdl1*-A upstream of *Pdl1*, and *Pdl1*-B, a putative FoxA1-binding sequence in the *Pdl1* promoter region (**Fig. 5f**).

We overexpressed FoxA1 in naive CD4$^+$ T cells and using ChIP found that FoxA1 bound to the *Pdl1*-B promoter site as compared to the housekeeping gene *Gapdh* (**Fig. 5g**). To exclude indirect binding, we performed FoxA1-binding electromobility shift assays (EMSA) with a probe containing the FoxA1-binding site but lacking the c-Fos–binding site of the control *Ttr* promoter[41] (*mTtr*). We incubated the labeled *mTtr* probe alone, with unlabeled *Pdl1*-A probe or with unlabeled *Pdl1*-B probe. The *Pdl1*-B but not the *Pdl1*-A probe competed with the *mTtr* probe for binding to FoxA1 (**Fig. 5h**). To confirm that *Pdl1*-B was the FoxA1-binding site in the *Pdl1* promoter, we labeled *Pdl1*-A and *Pdl1*-B probes separately. Supershifts showed that FoxA1 bound *Pdl1*-B and *mTtr* but not *Pdl1*-A (**Fig. 5i**). Co-transfection of cells with a luciferase reporter construct including the *Pdl1* promoter and a FoxA1-expressing vector resulted in increased luciferase activity, confirming that FoxA1 can bind to the *Pdl1* promoter (**Fig. 5j**).

RRMS responsiveness to IFN-β is associated with FoxA1$^+$ T_{reg} cells

We investigated whether clinical response to IFN-β treatment in patients with RRMS was associated with the generation of FoxA1$^+$ T_{reg} cells. We included 15 patients with RRMS that responded to IFN-β treatment (RRMS-R) and 9 patients that were non-responders (RRMS-NR)[42]. The RRMS-R patients experienced neither relapse nor progression after 2 years of IFN-β treatment, whereas the RRMS-NR patients showed relapses and increased disease progression (**Supplementary Fig. 11**). The percentage of FoxA1$^+$ T_{reg} cells in PBMCs were increased in the RRMS-R group as compared to baseline and the RRMS-NR group (**Fig. 6a–c**). We detected no expansion in the percentage of FoxA1$^+$ T_{reg} cells in the RRMS-NR patients. Only gated TCR-αβ$^+$CD4$^+$PD-L1^{hi} T cells from RRMS-R patients were positive for nuclear FoxA1, with a significant increase in the proportion of FoxA1$^+$ cells, investigated 24 months after entering IFN-β treatment (**Fig. 6d**). Next, we investigated whether FoxA1$^+$ T_{reg} cells isolated from RRMS-R patients treated with IFN-β are suppressive *ex vivo*. Purified FoxA1$^+$ T_{reg} cells from three additional RRMS-R patients treated with IFN-β inhibited T cell proliferation and induced ResT cell death (**Fig. 6e–g**).

DISCUSSION

Although T_{reg} cells are crucial in regulating many human inflammatory diseases[43], their relevance to favorable IFN-β responsiveness in patients with multiple sclerosis is under debate[8,9,12]. We anticipated that regulatory T cells suppress CNS-specific autoimmune inflammation. This idea led to the identification of a previously undescribed population of T_{reg} cells that express FoxA1 but not FoxP3. To our knowledge, this is the first report on the function of FoxA1 in T cells.

We have shown that expression of FoxA1 in $CD4^+$ T cells confers suppressive functions and a $FoxA1^+$ T_{reg} cell phenotype. Ectopic *FoxA1* expression led to FoxA1 nuclear localization. FoxA1 binds to the *Pdl1* promoter and induces Pd-l1 expression. $FoxA1^+$ T_{reg} cell–mediated suppression is dependent on PD-L1, which induces caspase 3–associated apoptosis. Although this mechanism of action has not been reported for T_{reg} cells, in myelodysplastic-syndrome cells, PD-L1 induces caspase 3–dependent apoptosis of T cells[44]. PD-L1–mediated suppression might be a common mechanism shared between $FoxA1^+$ T_{reg} cells and $FoxP3^+$ T_{reg} cells. Initially, *Pdl1*$^{-/-}$ and WT mice were shown to have similar numbers of T_{reg} ($CD4^+CD25^{hi}CD45RB^{lo}$) cells[45], but the role of Pd-l1 in the generation and function of T_{reg} cells has since been reported[46–48]. Pd-l1–mediated induction of T_{reg} cell development is associated with downregulation of pAkt-mTOR signaling and extracellular related kinase 2 (ERK2) but not p38 MAPK[48]. However, the signaling molecules altered by PD-L1–PD-1 in activated T cells are unclear. In $FoxA1^+$ T_{reg} cells, PD-L1 was required for suppression of responder T cell proliferation, inhibition of pAKT and phospho-p38 expression and induction of caspase 3–associated T cell apoptosis. We found no additional similarities between $FoxA1^+$ T_{reg} cells and n/iT_{regs} in terms of transcriptional profiles, cell surface markers or gene expression profiles. $FoxA1^+$ T_{reg} cells are negative for expression of FoxP3, cytotoxic T lymphocyte–associated protein 4 (CTLA4), TGF-β, IL-10 and IL-35 (refs. 49,50), which are all commonly associated with T_{reg} cells. The genetic signature of $FoxA1^+$ T_{reg} cells is distinct from those of their T cell progenitors, neuron-induced T_{reg} cells, n/iT_{reg} cells[28–31] and exhausted T cells[32].

$FoxA1^+$ T_{reg} cells generated by transfection of naive T cells with *FoxA1* downregulated pc-Fos and PD-L1 expression, were nonproliferative and exhibit suppressive function even long after *in vivo* transfer. FoxA1, a 'pioneer' factor, binds to chromatinized DNA directly, opens the chromatin and regulates target genes but can also enhance the binding of other cofactors to their target genes[51], such as GATA3 and T-bet[52]. Additional FoxA1 activity as an activator or repressor, its target genes in T cells and interaction with other factors remain to be determined.

IFN-β was sufficient to induce expression of FoxA1 and PD-L1, leading to $FoxA1^+$ T_{reg} cell generation. $nFoxA1^+$ T_{reg} cells and $iFoxA1^+$ T_{reg} cells share homology in their gene expression profiles. Additional pathways for IFN-β–IFNAR–mediated FoxA1 regulation may include activation of signal transducer and activator of transcription (STAT) molecules. STAT3 binds near the *Pdl1*-B site in tolerogenic APCs[53]; hence FoxA1 and STAT3 could interact to direct *Pdl1* transcription in T cells.

Our data demonstrate that FoxA1 establishes the $FoxA1^+$ T_{reg} cell lineage through modification of cell-surface and signaling molecules. Suppressive $FoxA1^+$ T_{reg} cells are also generated in association with favorable clinical outcomes to IFN-β treatment in patients with RRMS. These findings suggest that understanding the function of $FoxA1^+$ T_{reg} could lead to new therapies for inflammatory diseases.

METHODS

Methods and any associated references are available in the online version of the paper.

Accession codes. The microarray data generated in this publication have been deposited in NCBI's Gene Expression Omnibus (GEO) and are accessible through GEO series accession number GSE54490.

Note: Any Supplementary Information and Source Data files are available in the online version of the paper.

ACKNOWLEDGMENTS

This work was supported by grants from The Lundbeck Foundation in Denmark, The Danish Multiple Sclerosis Society, The Danish Council for Independent Research–Medical Sciences, The Danish Cancer Society, The Swedish Research Council–Medicine and the Bibi and Nils Jensen Foundation to S.I.-N. We thank H. Wekerle, U. Grohmann and M. Prinz for valuable discussion and suggestions.

AUTHOR CONTRIBUTIONS

Y.L. performed experiments, analyzed and prepared data for presentation and contributed to the writing of the manuscript. R.C. performed experiments and analyzed data and contributed to the writing of the manuscript. J.W., M.K., B.C., M.H. and X.W. performed experiments. M.K., B.C., M.H., X.W., M.C., X.M., M.H.D., F.S. and P.S.S. contributed to collection of patients' blood and clinical studies. K.H. contributed to discussions and final revision of the manuscript. S.I.-N. planned the study design, supervised the overall project, analyzed data and wrote the manuscript.

COMPETING FINANCIAL INTERESTS

The authors declare competing financial interests: details are available in the online version of the paper.

1. Josefowicz, S.Z., Lu, L.F. & Rudensky, A.Y. Regulatory T cells: mechanisms of differentiation and function. *Annu. Rev. Immunol.* **30**, 531–564 (2012).
2. Sundrud, M.S. & Nolan, M.A. Synergistic and combinatorial control of T cell activation and differentiation by transcription factors. *Curr. Opin. Immunol.* **22**, 286–292 (2010).
3. Yamane, H. & Paul, W.E. Early signaling events that underlie fate decisions of naive $CD4^+$ T cells toward distinct T-helper cell subsets. *Immunol. Rev.* **252**, 12–23 (2013).
4. Bach, J.F. Autoimmune diseases as the loss of active "self-control". *Ann. NY Acad. Sci.* **998**, 161–177 (2003).
5. Himmel, M.E., Yao, Y., Orban, P.C., Steiner, T.S. & Levings, M.K. Regulatory T-cell therapy for inflammatory bowel disease: more questions than answers. *Immunology* **136**, 115–122 (2012).
6. Kumar, V., Stellrecht, K. & Sercarz, E. Inactivation of T cell receptor peptide-specific CD4 regulatory T cells induces chronic experimental autoimmune encephalomyelitis (EAE). *J. Exp. Med.* **184**, 1609–1617 (1996).
7. Liu, Y., Teige, I., Birnir, B. & Issazadeh-Navikas, S. Neuron-mediated generation of regulatory T cells from encephalitogenic T cells suppresses EAE. *Nat. Med.* **12**, 518–525 (2006).
8. Korn, T. *et al.* Myelin-specific regulatory T cells accumulate in the CNS but fail to control autoimmune inflammation. *Nat. Med.* **13**, 423–431 (2007).
9. Viglietta, V., Baecher-Allan, C., Weiner, H.L. & Hafler, D.A. Loss of functional suppression by $CD4^+CD25^+$ regulatory T cells in patients with multiple sclerosis. *J. Exp. Med.* **199**, 971–979 (2004).
10. Dominguez-Villar, M., Baecher-Allan, C.M. & Hafler, D.A. Identification of T helper type 1-like, $Foxp3^+$ regulatory T cells in human autoimmune disease. *Nat. Med.* **17**, 673–675 (2011).
11. Astier, A.L., Meiffren, G., Freeman, S. & Hafler, D.A. Alterations in CD46-mediated Tr1 regulatory T cells in patients with multiple sclerosis. *J. Clin. Invest.* **116**, 3252–3257 (2006).
12. de Andrés, C. *et al.* Interferon β-1a therapy enhances $CD4^+$ regulatory T-cell function: an *ex vivo* and *in vitro* longitudinal study in relapsing-remitting multiple sclerosis. *J. Neuroimmunol.* **182**, 204–211 (2007).
13. Teige, I. *et al.* IFN-β gene deletion leads to augmented and chronic demyelinating experimental autoimmune encephalomyelitis. *J. Immunol.* **170**, 4776–4784 (2003).
14. Prinz, M. *et al.* Distinct and nonredundant *in vivo* functions of IFNAR on myeloid cells limit autoimmunity in the central nervous system. *Immunity* **28**, 675–686 (2008).
15. Liu, Y., Teige, I., Ericsson, I., Navikas, V. & Issazadeh-Navikas, S. Suppression of EAE by oral tolerance is independent of endogenous IFN-β whereas treatment with recombinant IFN-β ameliorates EAE. *Immunol. Cell Biol.* **88**, 468–476 (2010).

16. Teige, I., Liu, Y. & Issazadeh-Navikas, S. IFN-β inhibits T cell activation capacity of central nervous system APCs. *J. Immunol.* **177**, 3542–3553 (2006).
17. Hurtado, A., Holmes, K.A., Ross-Innes, C.S., Schmidt, D. & Carroll, J.S. FOXA1 is a key determinant of estrogen receptor function and endocrine response. *Nat. Genet.* **43**, 27–33 (2011).
18. Taube, J.H., Allton, K., Duncan, S.A., Shen, L. & Barton, M.C. Foxa1 functions as a pioneer transcription factor at transposable elements to activate Afp during differentiation of embryonic stem cells. *J. Biol. Chem.* **285**, 16135–16144 (2010).
19. Laganière, J. *et al.* Location analysis of estrogen receptor α target promoters reveals that FOXA1 defines a domain of the estrogen response. *Proc. Natl. Acad. Sci. USA* **102**, 11651–11656 (2005).
20. Li, Z. *et al.* Foxa1 and Foxa2 regulate bile duct development in mice. *J. Clin. Invest.* **119**, 1537–1545 (2009).
21. Motallebipour, M. *et al.* Differential binding and co-binding pattern of FOXA1 and FOXA3 and their relation to H3K4me3 in HepG2 cells revealed by ChIP-seq. *Genome Biol.* **10**, R129 (2009).
22. Kaestner, K.H. The FoxA factors in organogenesis and differentiation. *Curr. Opin. Genet. Dev.* **20**, 527–532 (2010).
23. Bernardo, G.M. & Keri, R.A. FOXA1: a transcription factor with parallel functions in development and cancer. *Biosci. Rep.* **32**, 113–130 (2012).
24. Lupien, M. *et al.* FoxA1 translates epigenetic signatures into enhancer-driven lineage-specific transcription. *Cell* **132**, 958–970 (2008).
25. Lucchinetti, C.F. *et al.* Inflammatory cortical demyelination in early multiple sclerosis. *N. Engl. J. Med.* **365**, 2188–2197 (2011).
26. Freeman, G.J., Wherry, E.J., Ahmed, R. & Sharpe, A.H. Reinvigorating exhausted HIV-specific T cells via PD-1–PD-1 ligand blockade. *J. Exp. Med.* **203**, 2223–2227 (2006).
27. Liu, Y. *et al.* PD-L1 expression by neurons nearby tumors indicates better prognosis in glioblastoma patients. *J Neurosci.* **33**, 14231–14245 (2013).
28. Hill, J.A. *et al.* Foxp3 transcription-factor–dependent and –independent regulation of the regulatory T cell transcriptional signature. *Immunity* **27**, 786–800 (2007).
29. Samstein, R.M. *et al.* Foxp3 exploits a pre-existent enhancer landscape for regulatory T cell lineage specification. *Cell* **151**, 153–166 (2012).
30. Fu, W. *et al.* A multiply redundant genetic switch 'locks in' the transcriptional signature of regulatory T cells. *Nat. Immunol.* **13**, 972–980 (2012).
31. Haribhai, D. *et al.* A central role for induced regulatory T cells in tolerance induction in experimental colitis. *J. Immunol.* **182**, 3461–3468 (2009).
32. Wherry, E.J. *et al.* Molecular signature of $CD8^+$ T cell exhaustion during chronic viral infection. *Immunity* **27**, 670–684 (2007).
33. Jain, J. *et al.* Normal peripheral T-cell function in c-Fos–deficient mice. *Mol. Cell Biol.* **14**, 1566–1574 (1994).
34. André, S., Tough, D.F., Lacroix-Desmazes, S., Kaveri, S.V. & Bayry, J. Surveillance of antigen-presenting cells by $CD4^+$ $CD25^+$ regulatory T cells in autoimmunity: immunopathogenesis and therapeutic implications. *Am. J. Pathol.* **174**, 1575–1587 (2009).
35. Porrini, A.M., De Luca, G., Gambi, D. & Reder, A.T. Effects of an anti–IL-10 monoclonal antibody on rIFNβ-1b–mediated immune modulation. Relevance to multiple sclerosis. *J. Neuroimmunol.* **81**, 109–115 (1998).
36. Zhang, X. *et al.* IFN-β1a inhibits the secretion of Th17-polarizing cytokines in human dendritic cells via TLR7 up-regulation. *J. Immunol.* **182**, 3928–3936 (2009).
37. Hesse, D. *et al.* Disease protection and interleukin-10 induction by endogenous interferon-β in multiple sclerosis? *Eur. J. Neurol.* **18**, 266–272 (2011).
38. Latchman, Y. *et al.* PD-L2 is a second ligand for PD-1 and inhibits T cell activation. *Nat. Immunol.* **2**, 261–268 (2001).
39. Butte, M.J., Keir, M.E., Phamduy, T.B., Sharpe, A.H. & Freeman, G.J. Programmed death-1 ligand 1 interacts specifically with the B7-1 costimulatory molecule to inhibit T cell responses. *Immunity* **27**, 111–122 (2007).
40. Ono, K. & Han, J. The p38 signal transduction pathway: activation and function. *Cell Signal.* **12**, 1–13 (2000).
41. Qian, X., Samadani, U., Porcella, A. & Costa, R.H. Decreased expression of hepatocyte nuclear factor 3α during the acute-phase response influences transthyretin gene transcription. *Mol. Cell. Biol.* **15**, 1364–1376 (1995).
42. Río, J. *et al.* Defining the response to interferon-β in relapsing-remitting multiple sclerosis patients. *Ann. Neurol.* **59**, 344–352 (2006).
43. Izcue, A., Coombes, J.L. & Powrie, F. Regulatory lymphocytes and intestinal inflammation. *Annu. Rev. Immunol.* **27**, 313–338 (2009).
44. Kondo, A. *et al.* Interferon-γ and tumor necrosis factor-α induce an immunoinhibitory molecule, B7-H1, via nuclear factor-κB activation in blasts in myelodysplastic syndromes. *Blood* **116**, 1124–1131 (2010).
45. Latchman, Y.E. *et al.* PD-L1–deficient mice show that PD-L1 on T cells, antigen-presenting cells, and host tissues negatively regulates T cells. *Proc. Natl. Acad. Sci. USA* **101**, 10691–10696 (2004).
46. Sandner, S.E. *et al.* Role of the programmed death-1 pathway in regulation of alloimmune responses *in vivo*. *J. Immunol.* **174**, 3408–3415 (2005).
47. Keir, M.E. *et al.* Tissue expression of PD-L1 mediates peripheral T cell tolerance. *J. Exp. Med.* **203**, 883–895 (2006).
48. Francisco, L.M. *et al.* PD-L1 regulates the development, maintenance, and function of induced regulatory T cells. *J. Exp. Med.* **206**, 3015–3029 (2009).
49. Collison, L.W. *et al.* The inhibitory cytokine IL-35 contributes to regulatory T-cell function. *Nature* **450**, 566–569 (2007).
50. Collison, L.W. *et al.* IL-35–mediated induction of a potent regulatory T cell population. *Nat. Immunol.* **11**, 1093–1101 (2010).
51. Jozwik, K.M. & Carroll, J.S. Pioneer factors in hormone-dependent cancers. *Nat. Rev. Cancer* **12**, 381–385 (2012).
52. Nakshatri, H. & Badve, S. FOXA1 in breast cancer. *Expert Rev. Mol. Med.* **11**, e8 (2009).
53. Wölfle, S.J. *et al.* PD-L1 expression on tolerogenic APCs is controlled by STAT-3. *Eur. J. Immunol.* **41**, 413–424 (2011).

ONLINE METHODS

Mice. *Ifnb*$^{-/-}$, *Ifnb*$^{+/-}$ and WT mice in a C57BL/10.RIII or C57BL/6 background (more than 20 generations backcrossed) were bred and kept at conventional animal facilities at the University of Copenhagen. *Ifnar* mice were from B&K Universal, UK. NOG (NOD.Cg*Prkdc*^{scid}*il2rg*^{tm1sug}/jicTac) and OT-II (B6.129S6-*Rag2*^{tm1Fwa}Tg/TcraTcrb/425 Cbn) mice were from Taconic and The Jackson Laboratory, respectively. Experiments were approved and performed in accordance with the national ethical committee (Animal Experiements Inspectorate under Danish Ministry of Food, Agriculture and Fisheries, The Danish Veterinary and Food Administration), approval number 2007/561-1364.

EAE induction and clinical evaluation. *Ifnb*$^{-/-}$ C57BL/10.RIII, *Ifnb*$^{+/-}$ C57BL/10.RIII heterozygous (HT) or WT littermates were used for active or adoptive EAE[13]. Gender- and age-matched mice were used in all experiments. Shortly, for adoptive-transfer EAE, male mice (8–12 weeks old) were irradiated (500 rad) and injected in the tail vein with a cell suspension of 2×10^6 $MBP_{89–101}$–specific T cells. Each mouse received co-transfer of either 2×10^6 $MBP_{89–101}$–specific T cells in 300 µl of PBS or purified FoxA1$^+$ T_{reg} cells. At days 0 and 2, each animal was given an intraperitoneal (i.p.) injection of 500 ng of pertussis toxin.

Active $MOG_{35–55}$–EAE in C57BL/6 *Ifnb*$^{-/-}$ and WT mice (gender- and age-matched) was induced as previously described[7]. Mice received an i.p. injection of mouse recombinant IFN-β (5,000 U) at days 0, 7 and 14 after immunization. Mice were blindly scored for clinical signs of EAE every day.

DTH response. Male mice, aged 8–15 weeks were immunized with 250 µg of $MBP_{89–101}$ emulsified in 50 µl of PBS and 50 µl of complete Freund's adjuvant. At day 13 after immunization, mice were injected with 100 µg of $MBP_{89–101}$ (in PBS) + FoxA1$^+$ T_{reg} cells (3×10^4 cells per ear) in the right ear or 100 µg of $MBP_{89–101}$ + $MBP_{89–101}$–specific T cells (3×10^4 cells per ear) in the left ear. Control mice received an injection of 100 µg of $MBP_{89–101}$ in the left ear and PBS + control T cells (3×10^4 cells per ear) in the right ear. The DTH response was measured as the difference in thickness (mm) between the right and left ears. Data for the group treated with control T cells are presented as (ear thickness after injection with $MBP_{89–101}$ + control T cells) – (ear thickness after injection with $MBP_{89–101}$). Data for the group treated with FoxA1$^+$ T_{reg} cells are presented as (ear thickness after injection with $MBP_{89–101}$ + FoxA1$^+$ T_{reg} cells) – (ear thickness after injection with $MBP_{89–101}$).

Preparation of CNS-infiltrating cells. At the indicated times after active EAE induction, brains and spinal cords were dissected, and infiltrating cells were isolated as described[7].

Real-time PCR. Standard procedures and analyses were followed[7]. Briefly, total RNA was isolated using a QIAGEN kit (QIAGEN), reverse transcribed into cDNA and amplified and quantified by SYBR Green (Bio-Rad) detection. Relative mRNA expression was calculated using glyceraldehyde 3-phosphate dehydrogenase (*Gapdh*) gene expression as an endogenous reference. The primers for *Pd-l1* were upper: 5′-CGC CCT TTT TAT TTA ATG TAT GGA-3′; lower: 5′-AAG TGA GGC GTC TGT GTT TGA G-3′. The primers for FoxA1 are listed in the **Supplementary Methods**.

Plasmids. FoxA1 was synthesized by Geneart into pMA with 5′ HindIII and 3′ Not I sites. FoxA1 was transferred to the mammalian expression vector pCDNA3.1 (Invitrogen) by standard cloning techniques.

Amaxa gene transfection. Purified CD4$^+$ T cells were transfected with pcDNA3.1 FoxA1 or control plasmid pcDNA3.1 using the Amaxa mouse T cell Nucleofector Kit (DPA-1007) (program X-001) according to the manufacturer's instructions. The transfection efficiency was evaluated by FoxA1 staining and FACS analysis.

Western blot analysis. Proteins were extracted from pcDNA3.1 FoxA1–transfected (FoxA1$^+$ T_{reg}) cells and pcDNA3.1-transfected (control T) cells. Standard procedures were followed[7]. Briefly, proteins were extracted in 40 µl SDS loading buffer (Invitrogen, USA). 30 µl of protein lysate was loaded on 4–12% SDS-PAGE gels, and proteins were blotted onto Hybond-C extra nitrocellulose membranes (GE Healthcare, UK). Rat anti-FoxP3 (FJK-16s, eBiosience, 1:2,000), goat anti-FoxA1 (ab5089, Abcam, 1:1,000), rabbit anti–pc-Fos (D82C12, Cell Signaling Technology, 1:1,000), rabbit anti–c-Fos (9F6, Cell Signaling Technology), rabbit anti-β-actin (13E5, Cell Signaling Technology, 1:3,000) and horseradish peroxidase (HRP)-conjugated secondary antibodies were used. The blots were developed using the enhanced chemiluminescence (ECL) technique (Millipore, MA, USA).

Immunohistochemistry. Brains and spinal cords of mice with EAE were dissected, embedded in optimal cutting temperature compound (OTC) (Sakura Finetek Denmark ApS, Værløse, Denmark) and snap frozen in isopentane on dry ice. Tissues were cryosectioned in 10-µm slices. Tissue sections were fixed in 4% paraformaldehyde (PFA) for 10 min and either stained with H&E or different antibodies and visualized by 3,3′-diaminobenzidine (DAB) as described[13]. Slides were visualized under light microscopy.

Affymetrix data analysis. We extracted RNA from FACSAria-sorted populations by TRIzol (Sigma), followed by DNaseI (Invitrogen) digestion with a subsequent TRIzol RNA purification. RNA was subjected to Affymetrix analysis, and data sets were quantile normalized and processed by the PLIER (Affymetrix) algorithm at 1.5-fold ($P \leq 0.05$).

The Affymetrix data (Mouse Genome 430 2) generated here, as well as published T_{reg} cell data from Affymetrix[28–31] (GSE7460, GSE14415, GSE9650 and GSE40685), were quantile normalized and summarized for each comparison using the justPlier implementation of the Plier algorithm in R. To draw heatmaps, the heatmap2 function from the gplots package in R was used. GSEA was performed using preprocessed data fed into the Java implementation of GSEA (v 2.0.12, Broad Institute) and analyzed with default settings (except for gene set permutation) using gene sets from MSigDb (v 3.1).

ChIP. ChIP was performed as described[54] with several modifications. Sonications were performed on a Bioruptor NextGen device (Diagenode) set for 30 s on, 30 s off for 12 cycles. Goat IgG (Sigma) was used as a negative control for the FoxA1-specific antibody (Abcam, ab5089), and 4 µg of each antibody was used. The ChIP-processed DNA was purified on a QIAquick PCR purification kit (Qiagen, 28104), and qPCR was performed with the Lightcycle 480 DNA SYBR Green I Master Mix (Roche). Primers for the selected sequences were designed using Primer3 (v. 0.4.0). qPCR primers for putative FoxA1 binding sites and control are listed in the **Supplementary Methods**.

EMSA. FoxA1-transduced 3T3-L1 cells were used to extract the nuclear fraction[55]. *Pdl1*-B was identified from the ChIP-seq peak data in ZR751 cells[17]. The precise location of the FoxA1 binding sequence was predicted using Clover and ContraV2. *Pdl1*-A and *Pdl1*-B EMSA probe sequences were selected from the genomic mm9 assembly (UCSC) and are within the amplicons of the *Pdl1*-A and *Pdl1*-B primer pairs used in the ChIP assay. EMSA was run as described previously[55]. The FoxA1-specific antibodies were 2F83 (05-1466, Millipore, 1 µg), which was used to verifiy the specificity of the results, and ab5089 (Abcam, 1 µg), which was used in supershift assays. The list of EMSA oligonucleotides used is contained in the **Supplementary Methods**.

Luciferase assay. 13,000 mycoplasma-tested, low-passage 3T3-L1 (ATCC CL-173) cells were reverse transfected with Lipofectamine 2000 (Invitrogen) in 96-well plates according to the manufacturer's recommendations with 10 ng pRLCMV (Promega), 95 ng pGL3 (Promega) and pCDNA3.1 (Invitrogen) or pCDNA3.1 FoxA1 mammalian expression plasmids. The medium was removed, 50 µl PBS was added to each well, and luciferase activity was measured according to the Dual-Glo Luciferase Protocol with 50 µl luciferase and *Renilla* substrate (Promega). Data were normalized to the activity of a pRLCMV internal control plasmid.

Patients. In total, 50 individuals were included: 27 patients with RRMS treated with IFN-β and 23 healthy controls.

24 patients with RRMS treated with IFN-β were included in the comparative study. Of these individuals, 15 were IFN-β responders (7 females, 8 males; mean age (s.d.): 34.3 (7.8) years), and 9 were IFN-β non-responders (7 females, 2 males; mean age: 37.1 (8.6) years). Patients with RRMS were classified as responders to IFN-β on the basis of the absence of relapses and no progression on the Expanded Disability Status Scale (EDSS) score during the first 2 years of treatment[42]. Patients were labeled as RRMS-NR when there was presence of relapses during the follow-up period: one or more relapses and an increase of at least 1 point in the EDSS score that persisted for at least two consecutive scheduled visits separated by a 6-month interval. Classification of patients with MS was done according to the methods of Lublin and Reingold[56]. The study was approved by the Hospital Universitari Vall d'Hebron Ethics Committee (PR(AG)32/2008).

Nine HCs (6 females, 3 males; mean age: 32.0 (6.0) years) were also included in the study. An additional three RRMS-R patients (all females, mean age: 29.3 (6.1) years) were recruited from the Danish MS Center in Copenhagen for fresh isolation of peripheral blood to be used in suppression assays. Patient blood was collected 36 h after IFN-β injection and subjected to FoxA1$^+$ T_{reg} cell isolation and suppressive studies, which were approved by the Scientific Ethics Committee for Copenhagen and Frederiksberg (protocol KF01-041/95). Additionally, buffy coats from 14 healthy individuals were included for functional studies. Informed consent was received from all individuals included in the study.

Blood sampling and PBMC isolation. Peripheral blood was collected by standard venipuncture into vacuum tubes with EDTA. PBMCs were isolated by Ficoll-Isopaque density gradient centrifugation (Gibco-BRL) and were freshly used or stored in liquid nitrogen until being used. PBMCs were collected at baseline and 24 months after IFN-β treatment. In HCs, longitudinal PBMCs were taken at two time points separated by 12 months ($n = 2$) and 24 months ($n = 7$). The study was approved by the Hospital Universitari Vall d'Hebron Ethics Committee (PR(AG)32/2008).

Human blood lymphocyte preparation. The buffy coats of blood donors or the blood of patients with MS (10–12 ml) was used for preparation of lymphocytes using Ficoll-Paque PLUS (7.5 ml) (GE Healthcare, 17-1440-02). The lymphocyte layer was collected and used for further studies.

siRNA-mediated silencing. Purified primary CD4$^+$ T cells from healthy donors were transfected with 100 nM of a PD-1–specific (predesigned siRNA directed against human PDCD1_3 FlexiTube siRNA (5 nmol), SI00071323, QIAGEN, sequence; CCCTGTGGTTCTATTATATTA) or Universal Negative Control 1/UNC siRNA (SIC001, Sigma-Aldrich) using the Amaxa Human T cells Nucleofector Kit (VPA-1002) (program U-014) according to the manufacturer's protocol.

Accell SMART pool siRNA specific to FoxA1 (combines four different siRNAs; E-046238-00; Dharmacon, Thermo Scientific) was introduced into purified mouse CD4$^+$ T cells according to the manufacturer's protocol. For non–off-target experiments, FoxA1 Accell SMART pool contained four siRNAs all targetting the 3′ UTR region. These four siRNAs were introduced separately or in pool to purified mouse CD4$^+$ T cells in the Accell delivery medium (B-005000-100, Thermo Scientific). Delivery efficiency and siRNA specificity were examined by intracellular staining of FoxA1. Accell nontargeting control siRNA (D-001910-01-05, Thermo Scientific) was utilized as a control. The siRNA sequences are listed in the **Supplementary Methods**. Pd-l1 Accell siRNA smart pool, mouse (E-040760-00-0010 nmol, Thermo Scientific) was used in some experiments.

FACS staining. Standard FACS procedures and analysis were previously described[7]. Shortly, after washing in FACS buffer (2% FCS in PBS), cells were incubated with Fc receptor–specific antibody (24.G.2, our hybridoma collection) at 10 μg ml^{-1}. Cells were then incubated with FACS antibodies (the list of antibodies and detailed information are included in the **Supplementary Methods**). For intracellular staining, cells were fixed and permeabilized using BD Cytofix/Cytoperm or using FoxP3-specific fixation and permeabilization solutions from the Human T_{reg} Flow Kit (FoxP3 Alexa Fluor 488/CD4 PE-Cy5/CD25 PE) (Biolegend, 320401) or Foxp3 staining buffer set (eBioscience). All antibodies were used at 1–5 μg ml^{-1} and were allowed to bind for 20 min on ice.

FoxA1$^+$ T_{reg} cell sorting from RRMS-R patients and *in vitro* IFN-β–induced FoxA1$^+$ T_{reg} cells. PBMCs were freshly prepared and then cultured with 1,000 U ml^{-1} of human recombinant IFN-β (PBL InterferonSource) for 72 h. For FoxA1$^+$ T_{reg} cell sorting from RRMS patients or PBMCs or from *in vitro* IFN-β–induced cells, lymphocytes were purified with the CD4$^+$ T Cell Isolation Kit II (Miltenyi Biotec, 130-091-155) and stained with antibodies to CD4, TCR and PD-L1 (the list of antibodies and detailed information are included in the **Supplementary Methods**) for 20 min at 4 °C in the dark. FoxA1$^+$ T_{reg} (TCR-αβ$^+$CD4$^+$PD-L1^{high}) cells were purified using a FACSAria sorting program.

Immunoflourescent cytochemistry. FoxA1$^+$ T_{reg} cells and FoxA1$^-$T (PD-L1^{lo} T) cells were generated using purified CD4$^+$ T cells treated with mIFN-β (100 U ml^{-1}) or hIFN-β (1,000 U ml^{-1}) for 48 h and then sorted with FACSAria and cultured in collagen (5005-B, Advanced BioMatrix, 1:44)-precoated chamber slides (177445, NUNC) for 5–6 h. For some experiments, pcDNA3.1 FoxA1–transfected and pcDNA3.1-transfected cells were used. Slides were subsequently stained with antibodies and visualized under a Zeiss fluorescence microscope.

The antibodies used were as follows: mouse FoxA1-specific antibody (Abcam, ab40868,1:500) and secondary Alexa Fluor 568 goat anti-mouse (A-11004, Invitrogen, 1:300) and rabbit anti–pc-Fos (5348, Cell Signaling Technology, 1:800) followed by Alexa Fluor 488–labeled secondary antibody (A-11029, Invitrogen, 1:300); biotin anti-mouse Pd-l1 (MIH5, eBiosience, 1:200), followed by secondary streptavidin-Cy3 (S7973-89J, US Biological, 1:300); and biotin hamster anti–TCR-β (H57-597, BD Biosciences, 1:200) and followed by Alexa Fluor 568 goat anti-hamster IgG (A-21112, Invitrogen, 1:300). DAPI (D3571, Invitrogen) was used for nuclei staining.

Suppression assays. Mouse FoxA1$^+$ T_{reg} cells, obtained from either mIFN-β (100 U ml^{-1})-treated (for 48 h) purified CD4$^+$ T cells from WT or *Ifnar*$^{-/-}$ mice, or purified CD4$^+$ T cells were transfected with pcDNA3.1 FoxA1 or control pcDNA3.1 or with FoxA1 siRNA or control siRNA. Human FoxA1$^+$ T_{reg} cells were obtained from hIFN-β (1,000 U ml^{-1})-treated purified CD4$^+$ T cells (for 48 h) or were purified from RRMS-R patients treated with IFN-β. Responder T cells (MACS-sorted CD4$^+$ T cells with the CD4$^+$ T Cell Isolation Kit II (Miltenyi Biotec, 130-091-155 for human, 130-095-248 for mouse) from either mouse spleens or the corresponding human peripheral blood) were labeled with CFSE and stimulated with plate-bound anti-mouse CD3 (550275, BD, 1 μg/ml) or anti-human CD3 (14-0037-82, eBioscience, 1 μg/ml) and soluble anti-mouse CD28 for 24 h (553295, BD, 10 μg/ml) or anti-human CD28 (CD28.6, eBiosience, 2 μg/ml). FoxA1$^+$ T_{reg} cells were purified by FACSAria and labeled with Texas Red tracker (Genovis) for some experiments. Suppressor and responder T cells were cocultured in a new culture plate without any antibody at a 1:1 ratio. After 24 h, cells were stained with violet dead cell marker (Invitrogen) or 7AAD and analyzed by FACS.

In vivo, chimeric mice were generated by transferring 1×10^6 CFSE-labeled, preactivated OT-II responder T cells to female NOG mice. 24 h later, these mice received WT or *Ifnar*$^{-/-}$ CD4$^+$ T cells transfected with either FoxA1 or control siRNA with or without an *in vivo* injection of mIFN-β (to generate FoxA1$^+$ T_{reg} cells *in vivo*). 24 h later, the suppression was assayed by FACS analysis of splenocytes for dilution of CSFE in gated responder T cells.

Statistical analyses. Statistical analyses were performed using GraphPad Prism 5. For details, see the figure legends and **Supplementary Methods**.

Additional Methods. Detailed methodology can be found in the **Supplementary Methods**.

54. Frank, S.R., Schroeder, M., Fernandez, P., Taubert, S. & Amati, B. Binding of c-Myc to chromatin mediates mitogen-induced acetylation of histone H4 and gene activation. *Genes Dev.* **15**, 2069–2082 (2001).
55. Carlsson, R., Thorell, K., Liberg, D. & Leanderson, T. SPI-C and STAT6 can cooperate to stimulate IgE germline transcription. *Biochem. Biophys. Res. Commun.* **344**, 1155–1160 (2006).
56. Lublin, F.D. & Reingold, S.C. Defining the clinical course of multiple sclerosis: results of an international survey. National Multiple Sclerosis Society (USA) Advisory Committee on Clinical Trials of New Agents in Multiple Sclerosis. *Neurology* **46**, 907–911 (1996).

doi:10.1038/nm.3485